Functional characterization of rare variants of SCHAD, a protein involved in unregulated insulin secretion

Henrikke Nilsen Hovland

This thesis is submitted in partial fulfilment of the requirements
for the degree of Master of Science

Department of Biological Sciences and
Gade Laboratory for Pathology,
Department of Clinical Medicine
University of Bergen

June 2018

Table of Contents

Acknowledgements

The work presented in this thesis was carried out during the period of August 2017 to May 2018, primarily at Gade Laboratory for Pathology, Department of Clinical Medicine, University of Bergen and at Center for Medical Genetics and Molecular Medicine, Haukeland University Hospital.

First, I would like to thank my main supervisor Anders Molven for his brilliant guidance and suggestions throughout my project, and for letting me be a part of his research group. I am also deeply indebted to my co-supervisor Kelly Velasco for excellent teaching in the lab, supervision of my experimental and written work, and for patiently answering all my questions. The help from both of you has been highly appreciated, and I have really enjoyed being able to work on such an interesting topic.

I also want to thank Åsta Ottesen, Solrun Steine, Karianne Fjeld, Johanna Lüdeke and Benedict Man Hung Choi for their technical support and assistance in laboratory experiments related to the SCHAD project, and Janne Molnes for sharing her experience in pathogenic classification of human genetic variants. I am grateful to everyone at the KG Jebsen Center for Diabetes Research for providing such an enthusiastic scientific environment.

Thanks to Åsta and my master fellow student Ranveig Seim Brekke for your good company in the lab, in our office, and for all the fun lunch breaks.

Finally, thanks to my friends and family for always being supportive and encouraging.

Henrikke Nilsen Hovland
May 2018

Abbreviations

aa	Amino acids
ADA	American Diabetes Association
ADP	Adenosine Diphosphate
α-KG	α-ketoglutarate
ATP	Adenosine Triphosphate
BCA assay	Bicinchoninic Acid assay
bp	Base pair
BSA	Bovine Serum Albumin
CHI	Congenital Hyperinsulinism of Infancy
Co-A	Coenzyme A
ddH2O	Double deionized water
DMEM	Dulbecco's Modified Eagle's Medium
DMSO	Dimethyl Sulfoxide
DNA	Deoxyribonucleic Acid
dNTP	Deoxyribonucleotide Triphosphate
DTT	Dithiothreitol
E. coli	*Escherichia coli*
EDTA	Ethylenediaminetetraacetic Acid
FAO	Fatty Acid Oxidation
FBS	Fetal Bovine Serum
FT	Flow Through
g	G-force
GDH	Glutamate Dehydrogenase
GLUD1	Glutamate Dehydrogenase 1 gene
HADH	Short-chain L-3-Hydroxyacyl-CoA Dehydrogenase gene
HBS	HEPES-Buffered Saline
HEK293	Human Embryonic Kidney cell line 293
HRP	Horseradish Peroxidase
kb	Kilo bases
kDa	Kilo Daltons
KO	Knock Out
LB medium	Lysogeny Broth medium
mAu	Milli Absorbance unit
MBP	Maltose-Binding Protein
µg	Microgram
µl	Microliter
MODY	Maturity-Onset Diabetes of the Young
mqH_2O	Milli-Q water
MW	Molecular Weight
NAD	Nicotinamide Adenine Dinucleotide
PBS	Phosphate Buffered Saline
PCR	Polymerase Chain Reaction

RCF	Relative Centrifugal Force
RIPA buffer	Radioimmunoprecipitation Assay buffer
RNA	Ribonucleic Acid
Rpm	Revolutions per minute
RT	Room Temperature
RT-PCR	Reverse Transcription Polymerase Chain Reaction
*S*CHAD	Short-Chain L-3-Hydroxyacyl-CoA Dehydrogenase protein
SDS-PAGE	Sodium Dodecyl Sulfate Polyacrylamide Gel Electrophoresis
SN	Supernatant
SNP	Single-Nucleotide Polymorphism
SOC medium	Super Optimal broth with Catabolite repression
TCA cycle	Tricarboxylic Acid cycle
WT	Wild Type

Abstract

Congenital Hyperinsulinism of Infancy (CHI) is a group of rare inherited disorders characterized by persistent hypoglycaemia due to inappropriate elevated secretion of insulin from the pancreatic beta cells. CHI can be caused by abnormalities in at least 10 genes. One of them, *HADH*, encodes the mitochondrial enzyme SCHAD, which has two functions: it catalyses the third step in the oxidation of fatty acids, and it has been reported to negatively regulate the enzyme glutamate dehydrogenase (GDH). Inactivating mutations in *HADH* lead to a loss of the inhibitory protein interaction of SCHAD, which then cause increased insulin secretion due to overactive GDH.

We here aimed to understand the functional impact of rare SCHAD variants present in human populations. We have explored the effect of four pathogenic SCHAD variants with regard to the level of expression, subcellular localization and enzymatic activity. Two of the variants (G34R and I184F) showed protein instability and had clearly reduced level of protein expression in HEK293 cells. The mRNA levels appeared normal, which indicated that the cause of instability lies downstream of the transcription. The two other variants (K136E and M188V) had normal protein expression levels in HEK293 cells, but a severely reduced enzymatic activity compared to the wild type protein. The four SCHAD mutations did not affect the mitochondrial localization of the protein. In addition to the four pathogenic variants, protein stability of 11 other rare SCHAD variants was tested in HEK293 cells by the use of the protein synthesis inhibitor cycloheximide. Four additional variants were found to be unstable (I33M, H170R, P258 and G303S). The effect of the different SCHAD variants on GDH interaction was evaluated by co-immunoprecipitation. Protein:protein interaction could be detected for the SCHAD wild type protein, whereas several of the other variants seemed to have reduced or lost binding to GDH. The data gathered throughout the study were in combination with other relevant information used to reclassify the pathogenicity of a total of 16 rare SCHAD variants present in human populations. Taken together, our results illustrate the extensive work necessary for evaluating the functional impact of rare variants that are identified in high-throughput sequencing of human genomes.

1. Introduction

1.1 The endocrine pancreas

The pancreas is a digestive gland located posteriorly to the stomach, between the duodenum and the spleen (Figure 1.1A) [1]. The organ can be divided into two functional compartments: the endocrine and the exocrine pancreas. The exocrine pancreas constitutes the major part of the organ and contains acinar and ductal cells producing digestion enzymes and bicarbonate, respectively, which are secreted into the duodenum as pancreatic juice. The endocrine pancreas regulates energy metabolism by producing the hormones insulin, glucagon, and somatostatin [2]. The project described in this thesis concerns the endocrine elements, which will therefore be the focus of the introduction.

1.1.1 The islets of Langerhans

The endocrine pancreas consists of approximately 1 million cell clusters called the islets of Langerhans (Figure 1.1B). These clusters constitute 1-2% of the pancreas [2]. The islets contain four major cell types: beta (54%), alpha (35%), delta (11%) and gamma/pancreatic polypeptide cells (a few percent) [3]. The different endocrine cell types produce hormones that mainly serve to coordinate responses to maintain glucose homeostasis. The beta cells produce insulin, the alpha cells produce glucagon, the delta cells secrete somatostatin, and the polypeptide cells secrete vasoactive intestinal peptide [2]. The islets are intimately connected to the vasculature, which allow them to effectively secrete hormones into the blood in response to environmental changes [4].

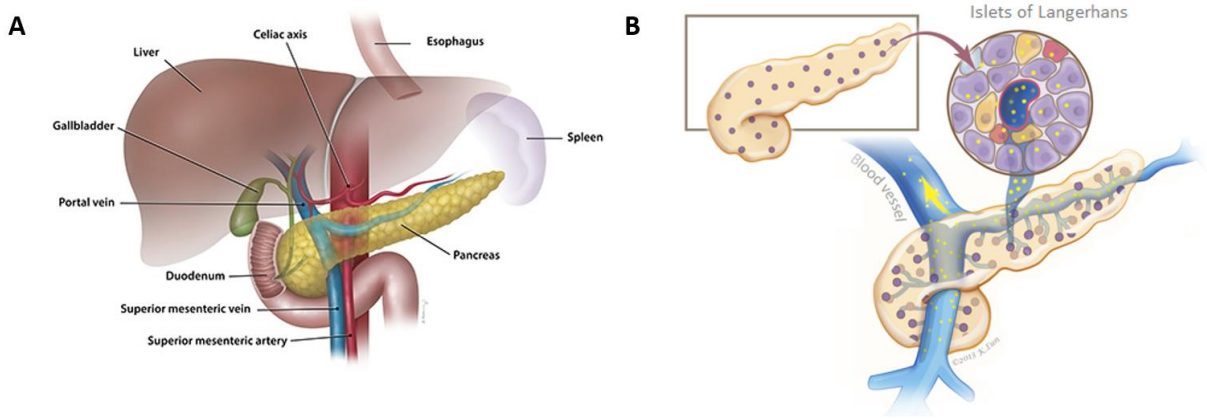

Figure 1.1 – Structure and function of the human pancreas. **A)** The pancreas (yellow) is located in the abdomen, with the duodenum on the right side and the spleen on the left. Other surrounding organs and major vessels are also shown. Figure from [5]. **B)** The islets of Langerhans are scattered throughout the pancreas. The endocrine cells produce glucose-regulating hormones that are released into the blood stream. Figure adapted from [6].

1.1.2 Regulation of insulin secretion

Insulin secreted from the beta cells is the main regulator of blood glucose level, ensuring that it is in balance with the body's feeding state. During food intake, i.e. when blood sugar rises, the beta cells sense this change and secrete insulin into the blood stream in corresponding amounts. This enables striated muscle cells and adipocytes to absorb the glucose and use it as energy. Excess glucose is stored in the liver and muscles as glycogen through the process known as glycogenesis, and can be released at times of energy shortage [2]. Insulin also stimulates storage of excess fuel as fat in adipose tissue [7].

Glucagon secreted from the alpha cells has the opposite effect of insulin on the blood glucose level, as shown in Figure 1.2. Thus, whereas insulin lowers the level of blood glucose, glucagon increases it [8]. These hormones thereby work together to maintain appropriate blood glucose levels, which normally are in the range of 3.5-5.5 mmol/L in humans [9]. Glucagon signalling results in the net output of glucose from the liver through glycogen breakdown, gluconeogenesis (conversion of protein to glucose) and inactivation of glycogen synthesis. In addition, it mobilizes an alternative source of energy by promoting the reduction of fatty acids from adipose tissue [7].

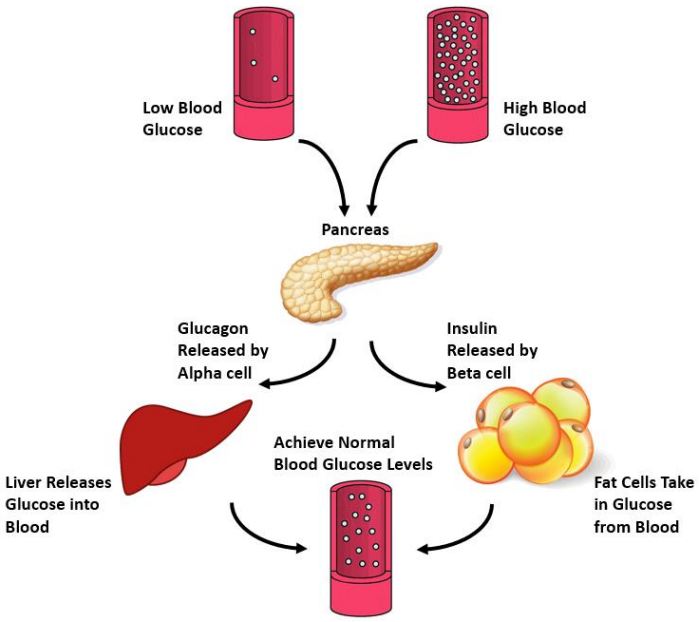

Figure 1.2 – Opposing effects of insulin and glucagon in the regulation of blood glucose. Insulin and glucagon work together to maintain blood glucose levels within a normal range. When blood glucose is high, insulin is released from the pancreatic beta cells. Insulin stimulates the uptake of glucose into cells in a variety of tissues, here exemplified by adipose tissue. When blood glucose is low, glucagon is released from the pancreatic alpha cells. Glucagon serves to raise the glucose level in the blood. Figure based on [10].

Insulin is also secreted from the beta cells in response to additional nutrients such as other monosaccharides, amino acids and free fatty acids. However, the response to glucose is the strongest. Several hormones like melatonin, estrogen, leptin, growth hormone and glucagon like peptide-1 affect the regulation of insulin secretion [4].

Insulin is stored in secretory granules within the beta cells, and is released through the fusion of these granules with the plasma membrane [2]. The main steps in the pathway of insulin secretion are shown in Figure 1.3. After glucose has entered the beta cells, it is converted to pyruvate through glycolysis. Pyruvate is then metabolized to acetyl-CoA, which is oxidized in the mitochondria by the tricarboxylic acid cycle (TCA cycle) to produce ATP [4]. The rise in ATP concentration initiates the closure of the K_{ATP} channels in the beta cell plasma membrane, reducing the efflux of potassium (K^+), which in turn causes the depolarization of the cell membrane. The depolarization triggers opening of voltage-gated calcium (Ca^{2+}) channels, and leads to an influx of Ca^{2+} into the cell [11]. The increase in intracellular Ca^{2+} concentration is the primary insulin secretory signal [4] that initiates the exocytosis of insulin from the secretory granules [11].

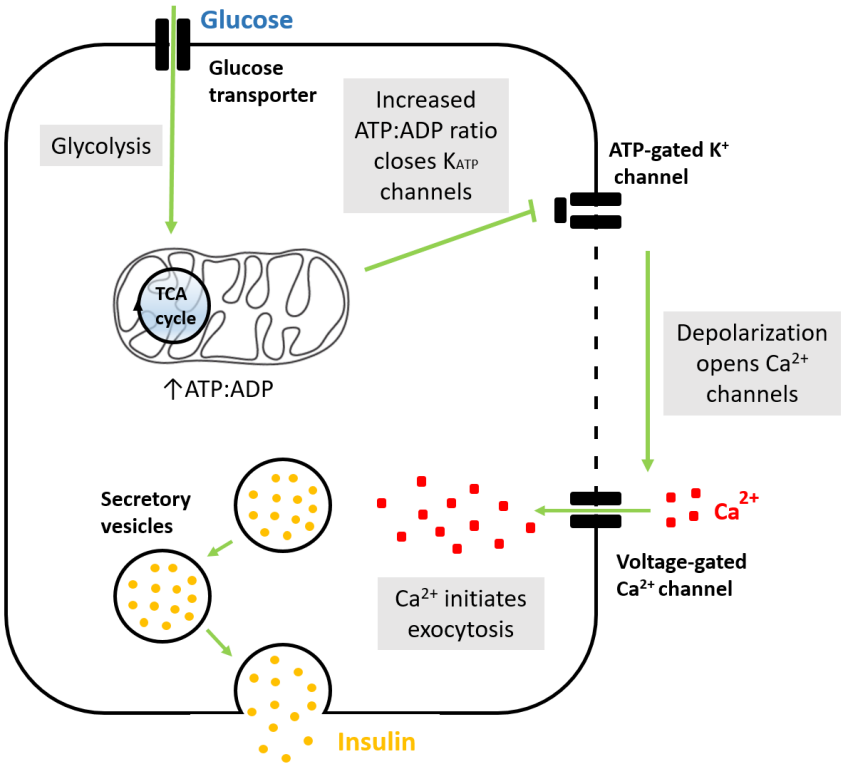

Figure 1.3 – Main steps in the pathway of insulin secretion. Glucose metabolism in the pancreatic beta cells results in an increased ATP:ADP ratio, which leads to closure of ATP-gated K^+ channels. Depolarization of the beta cell membrane leads to opening of voltage-gated Ca^{2+} channels. Increased intracellular Ca^{2+} concentration initiates exocytosis of insulin from secretory granules. Drawn on the basis of [12].

1.1.3 Diabetes

Insulin is required to maintain normal energy metabolism [4]. Defects in the secretion and/or action of insulin can lead to diabetes, which is the most common disease that involves the pancreas. Diabetes is a group of metabolic disorders where the hallmark is chronic hyperglycaemia, i.e. a fasting blood glucose level above 7 mmol/L [2].

According to the American Diabetes Association (ADA), diabetes can be classified into four main categories: type 1 diabetes, type 2 diabetes, gestational diabetes mellitus, and specific types of diabetes due to other causes, like monogenic diabetes syndromes [13].

Type 1 diabetes is caused by cell-mediated autoimmune destruction of the pancreatic beta cells. This form accounts for 5-10% of all diabetes cases. As the disease proceeds, at a rate according to the rate of beta cell destruction, the patients will have little or no remaining insulin secretion, and they therefore become completely dependent on treatment with insulin for survival. Type 1 diabetes typically has a juvenile onset, but can also occur in adults. The disease is defined by the presence of autoimmune markers [13].

Type 2 diabetes is the most prevalent form of diabetes and accounts for around 90% of all cases. Although the disease is commonly known as “lifestyle diabetes”, it also has a strong genetic component. Type 2 diabetes typically has an adult onset, and the risk of developing the disease increases with obesity and lack of physical activity. The disease is defined by a combination of relative insulin deficiency (inadequate response) and a peripheral insulin resistance [13]. A loss of beta cells mass and function, in addition to dysfunction in insulin secretion, makes the beta cells unable to secrete enough insulin to compensate for the decrease in insulin sensitivity in the patients. [4] Since there is no autoimmune destruction of the beta cells, many of the patients can manage their disease by interventions in diet and lifestyle. Nevertheless, oral medications are often needed and some patients eventually become insulin-dependent [13].

Gestational diabetes mellitus (GDM) can appear in women in their second or third trimester of pregnancy. The diagnosis is given if there was no diabetes before the pregnancy. Normal glucose level in usually restored when the baby is born. However, GDM increases the risk of type 2 diabetes later in life [13].

Monogenic diabetes is a group of diseases caused by around 20 single-gene defects that affect the development of the pancreas or the physiology of the beta cell [14]. Monogenic diabetes syndromes include neonatal diabetes and maturity-onset diabetes of the young (MODY). The monogenic forms account for somewhere between 1% and 5% of all diabetes cases. Neonatal diabetes appears before the age of 6 months, and can be transient or permanent. Overexpression of genes on chromosome 6p24 leads to the transient type, while autosomal dominant mutations in the two genes that encode the subunits of the K_{ATP} channels in the beta cells (*KNCJ11* and *ABCC8*) result in permanent neonatal diabetes. MODY is characterized by impaired insulin secretion, with minimal or no defects in insulin action. The disease is inherited in an autosomal dominant pattern most commonly caused by abnormalities in the genes *GCK*, *HNF1A* and *HNF4A* [13].

Other causes of diabetes included in the ADA classification are diseases of the exocrine pancreas (e.g. cystic fibrosis- or pancreatitis-related diabetes) and drug- or chemical-induced diabetes [13].

1.2 Congenital hyperinsulinism of infancy

1.2.1 Definition and phenotype

Congenital hyperinsulinism of infancy (CHI) is a group of inherited disorders characterized by hypoglycaemia and inappropriately elevated secretion of insulin [12]. Thus, insulin is secreted from the beta cells even though the blood glucose level is low, and CHI can be considered as the opposite condition of diabetes. The unregulated secretion of insulin leads to inhibition of gluconeogenesis, fatty acid oxidation and ketogenesis. CHI therefore prevents the brain from all sources of fuel [15]. Some affected children have high birth weight due to high insulin secretion also in utero.

CHI has an incidence of around 1 in 50 000 births, but it is more frequent (up to 1:2500) in areas with high rates of consanguinity [16].

1.2.2 Molecular causes

During the last two decades, abnormalities in at least 10 genes have been described to cause CHI, all of which are involved in the regulation of insulin secretion [11]. The gene defects can be divided into three main groups. The first is designated channelopathies and arise from mutations in genes that encode the two subunits of the K_{ATP} channels in the beta cells (*ABCC8* and *KCNJ11*, both located on chromosome 11) [17, 18]. The second group consists of metabolopathies, in which the underlying defect is dysregulated metabolic pathways. These are much rarer than the channelopathies [19]. The third group includes genes that encode transcription factors.

1.2.2.1 Channelopathies causing CHI

Inactivating mutations in the ion channel genes *ABCC8* and *KCNJ11* cause the most severe forms of CHI. [17, 18]. *ABCC8* encodes the sulfonylurea receptor 1 protein (SUR1), while *KCNJ11* encodes the inward rectifier K^+ channel Kir6.2. The K_{ATP} channel of the pancreatic beta cell consists of eight subunits, four of each of these two proteins, as shown in Figure 1.4A. The main role of SUR1 is to regulate the activity of Kir6.2, which is the pore-forming unit that enables the flow of K^+ ions. The K_{ATP} channels sense the level of ATP in the beta cells and are inhibited by high levels. Inactivating mutations that cause defective K_{ATP} channels will lead to a persistent depolarization of the beta cell membrane, opening of voltage gated calcium channels, and hence unregulated insulin secretion (Chapter 1.1.2) [11]. Mutations in the *ABCC8* gene are by far the most common cause of CHI [20, 21].

Histologically, CHI caused by K_{ATP} mutations can be divided into two major forms: focal and diffuse. In focal CHI (30-40% of all channel CHI cases) only localized parts of the pancreas are affected by the disease, and the surrounding parenchyma cells appear normal. Focal CHI is result of a paternally inherited mutation in the K_{ATP} channels, followed by a somatic loss of heterozygosity affecting the normal maternal allele. In diffuse CHI (60-70% of all channel CHI cases), the gene defect is present in all cells, implying that all islets are abnormal [11].

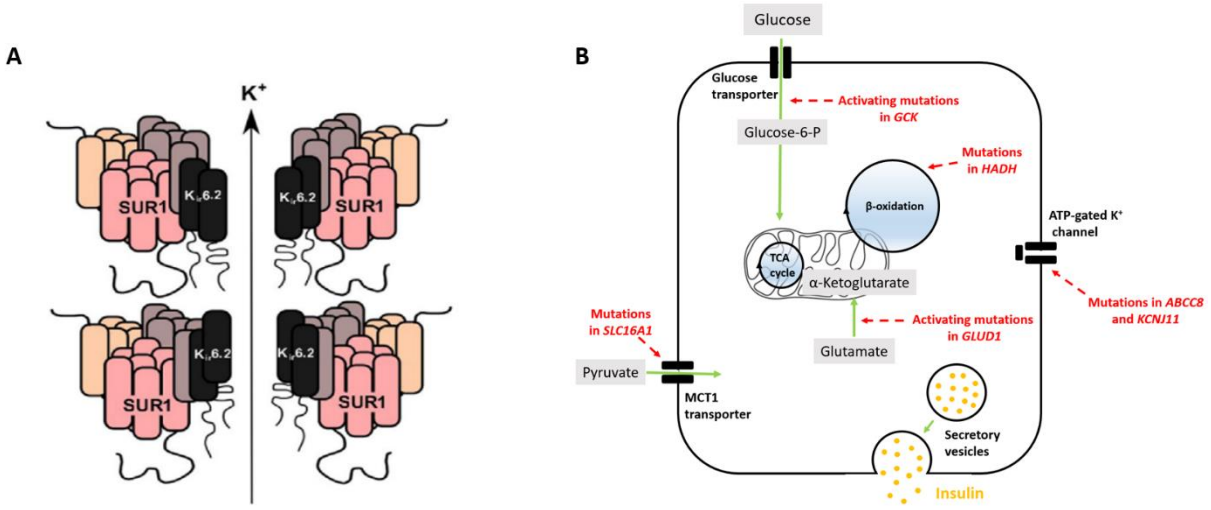

Figure 1.4 – Molecular causes of CHI. **A)** The ATP-gated K^+ channels of the pancreatic beta cell consist of four SUR1 and four Kir6.2 protein subunits. Figure from [11]. **B)** Summary of some of the genetic defects causing CHI. Figure drawn after [12].

1.2.2 Metabolopathies causing CHI

The known CHI genes encoding metabolic enzymes are *GLUD1*, *GCK*, *SLC16A1*, *UCP2*, *HK1* and *HADH*. *GLUD1* encodes the metabolic enzyme glutamate dehydrogenase (GDH). GDH catalyses a reversible reaction that converts glutamate to α-ketoglutarate, which enters the TCA cycle resulting in production of ATP in the beta cell. Activating mutations in *GLUD1* will therefore result in too much ATP and enhanced insulin secretion [11]. This is the second most common form of CHI after the channelopathies. It has a dominant inheritance pattern [22, 23].

GCK encodes the enzyme glucokinase, which is responsible for converting glucose to glucose-6-phosphate in the first activating step of the glycolytic pathway. Dominant activating mutations in *GCK* will increase the concentration of activated glucose inside the cell, and thereby lower the glucose threshold for release of insulin [11, 24]. This is the third most common cause of CHI [25].

HK1 encodes the enzyme hexokinase 1, which similarity to glucokinase catalyses the first step in the metabolism of glucose. *HK1* expression is normally silenced in the beta cells, but activating mutations can lead to inappropriate activation of hexokinase in the islets. This will cause secretion of insulin at lower glucose levels than normal, and thus cause CHI [9, 26].

SLC16A1 encodes the monocarboxylate transporter 1 (MCT1), a protein responsible for regulating the transport of lactate and pyruvate into the beta cells. Under normal conditions the transporter is not expressed in the beta cells to prevent hypoglycaemia during heavy exercise, but gain-of-function mutations can enable its expression also in these cells. Increased transport of pyruvate results in higher ATP levels, which again inhibit the K_{ATP} channels and lead to CHI [11]. Specific for this form of CHI is that the patients experience exercise-induced hypoglycaemia [27]. During anaerobic exercise, the produced lactate will enter the TCA cycle together with pyruvate and result in production of ATP [11].

UCP2 encodes the mitochondrial uncoupling protein 2 (UCP2). UCP2 functions by mediating leakage of protons across the inner mitochondrial membrane, thereby inhibiting the generation of ATP and subsequently the secretion of insulin [9]. Loss-of-function mutations release this uncoupling and may enhance the oxidation of glucose in the beta cell to a degree sufficiently for CHI to develop [11, 28].

The final CHI gene that encodes a metabolic enzyme, *HADH*, will be the focus of Chapter 1.3.

1.2.2.3 Defects in genes encoding transcription factors that cause CHI

This third group of CHI genes encode the transcription factors hepatocyte nuclear factor 1 alpha (*HNF1A*) and hepatocyte nuclear factor 4 alpha (*HNF4A*). Mutations in these genes can lead to a transient form of CHI with a highly heterogeneous phenotype. *HNF1A* encodes a transcription factor that enhances the expression of several pancreatic genes. Heterozygous loss-of-function mutations can lead to CHI with a relatively mild phenotype. Some of the patients later progress to develop MODY3 diabetes [11]. *HNF4A* regulates several genes involved in insulin secretion. Dominant inactivating mutations in *HNF4A* may lead to a more severe form of CHI. Patients with this form of CHI will eventually develop MODY1 diabetes [11]. Since mutations in *HNF1A* and *HNF4A* are associated with the development of diabetes later in life, an accurate molecular diagnosis is important to ensure appropriate surveillance. The molecular causes of CHI are summarized in Figure 1.4B and Table 1.1.

Table 1.1 – Molecular causes of CHI. D = autosomal dominant inheritance, R = autosomal recessive inheritance, IM = inactivating mutations, AM = activating mutations.

Group	Gene	Encoded Protein	Inheritance	Mutation type
Channelopathies	*ABCC8*	Sulfonylurea receptor 1 (SUR1)	D/R	IM
	KCNJ11	Inward rectifier K^+ channel Kir6.2	D/R	IM
Metabolopathies	*GLUD1*	Glutamate dehydrogenase (GDH)	D	AM
	GCK	Glucokinase (GCK)	D	AM
	HADH	Short chain L-3-hydroxyaxyl-CoA dehydrogenase (SCHAD)	R	IM
	SLC16A1	Monocarboxylate transporter 1 (MCT1)	D	AM
	UCP2	Mitochondrial uncoupling protein 2 (UCP2)	D	AM
	HK1	Hexokinase (HK1)	D	AM
Transcription factor genes	*HNF1A*	Hepatocyte nuclear factor 1 alpha (HNF1A)	D	IM
	HNF4A	Hepatocyte nuclear factor 4 alpha (HNF4A)	D	IM

1.2.3 Treatments of CHI

In most cases, the phenotype of CHI becomes apparent within a few days or weeks after birth. If not treated, the unregulated insulin secretion can lead to severe hypoglycaemia. This is a critical condition as the brain is especially vulnerable during the first years of development, and glucose is the main fuel of the brain. A delay in diagnosis and lack of treatment in the neonatal period can therefore cause permanent brain damage or, in worst-case scenarios, even death [9]. Genetic mutation testing/screening of children with hypoglycaemia, when CHI is suspected, is important for early diagnosis, determination of the cause of disease, and implementation of the optimal treatment. This is vital to ensure the best possible outcome for the patient [29].

Diazoxide is the most common medical treatment in CHI and is usually the first treatment tested when a child is diagnosed with the disease. Diazoxide is a K_{ATP} channel agonist that stimulates the channels to remain open and hence suppresses the release of insulin [29]. However, diazoxide will only be effective in cases where there is no defect in the K_{ATP} channels. If the channels are affect, octreotide is a treatment option that inhibits the release of insulin downstream of the K_{ATP} channels by binding to somatostatin receptors [9, 29].

Patients with K_{ATP} mutations are often unresponsive to drug treatment because the K_{ATP} channels are either defective or absent [11]. Regulated food intake and tube feeding can be helpful in some cases. If medications do not give the appropriate response, a partial or subtotal surgical removal of the pancreas may be needed [12]. Subtotal pancreatectomy will in most cases eventually result in diabetes and exocrine insufficiency, and should therefore be avoided if not absolutely necessary [11].

In the case of K_{ATP} mutations, it is particularly important to distinguish between focal and diffuse cases. This is because removal of a localized lesion can cure the patient [30]. Identification of focal lesions are now done by ^{18}F-fluoro-L-dihydroxyphenylalanine (^{18}F-DOPA) PET scans [29].

1.3 SCHAD deficiency as cause of CHI

1.3.1 Discovery and phenotype

Short-chain L-3-hydroxyacyl-CoA dehydrogenase (SCHAD) deficiency is a rare cause of CHI, and was first discovered by Clayton et al. in 2001 [31] when examinations of an infant with episodes of hypoglycaemia showed elevated blood level of 3-hydroxybutyryl-carnitine (a fatty acid metabolite). This led to activity measurements of fatty acid oxidation (FAO) enzymes, of which the enzyme SCHAD showed a clearly reduced activity. Sequencing of the SCHAD encoding gene (*HADH*) discovered an inactivating mutation [31]. This was the first time an enzyme from the FAO pathway was directly connected to CHI. At the time, the role of the observed *HADH* mutation as the cause of CHI was regarded with some scepticism, and it was speculated that there was an additional unidentified mutation that explained the disease.

In 2004, Molven et al. finally established SCHAD deficiency as a cause of CHI [32]. A whole-genome scan with microsatellite markers of a consanguineous family with four cases of CHI pinpointed the mutated gene to chromosome 4, and a disrupted splice site in exon 5 of *HADH* was then revealed in affected subjects. Like the patient reported by Clayton et. al, these individuals also showed reduced SCHAD activity, and increased blood 3-hydroxybutyryl-carnitine concentration [32]. In 2016, Molven et al. transplanted islets from global SCHAD KO (knock out) mice into mice with induced diabetes, and showed that hypoglycaemia in SCHAD-CHI is islet cell-autonomous [33].

Abnormal levels of fatty acid metabolites, namely increased concentration of 3-hydroxybuturyl in blood and 3-hydroxyglutaric acid in urine, are characteristics of SCHAD-deficiency [32, 33]. In contrast to many other CHI forms, affected children have normal birth weights, and even though SCHAD participates in the degradation of fatty acids, no phenotypic features of fatty acid oxidation disorders (hepatic dysfunction, cardiomyopathy or skeletal muscle affection) are seen [34].

1.3.2 The *HADH* gene

The gene coding for the SCHAD protein is located on chromosome 4q22-26 (Figure 1.5A) and is known as *HADH* (hydroxyacyl-CoA dehydrogenase). In databases such as UniProt (https://www.uniprot.org), NCBI (https://www.ncbi.nlm.nih.gov) and Ensembl (https://www.ensembl.org), there are at least three protein coding transcript variants reported, which are produced by alternative splicing. The encoded isoforms have a length of 331, 318 and 314 amino acids (aa) (Figure 1.5B). The 314 aa isoform (reference sequence NM_005318.43) used in this study is the most well-characterized one and considered as the main form. The variant encoding this isoform is lacking the exon 7, as illustrated in Figure 1.6. There is little or no biological information about the other variants.

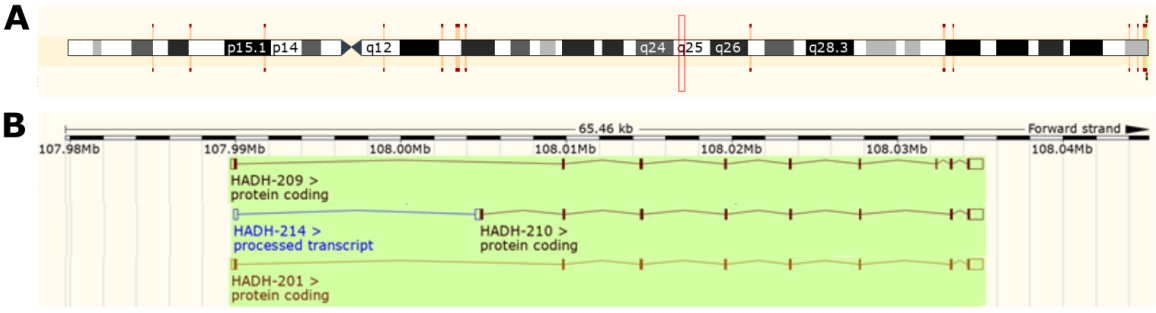

Figure 1.5 – Location, structure and transcript variants of the *HADH* gene. A) *HADH* is located on chromosome 4q22-26, as shown by the red box. **B)** Comparison of three protein coding transcript variants of *HADH*. The encoded isoforms have a length of 331 (*HADH*-209), 318 (*HADH*-210) and 314 aa (*HADH*-201). The bars represent the exons and the lines are the intronic regions. The image was obtained from the Ensembl browser (https://www.ensembl.org/Homo_sapiens/Gene/Summary?g=ENSG00000138796;r=4:107989714-108035175)

1.3.3 The SCHAD protein structure

The SCHAD protein has a 314 aa with the first 12 aa constituting a mitochondrial import signal. This signal directs the protein to the mitochondrial compartment, and is cleaved while the protein is translocated. The mature SCHAD protein has two domains: a NAD^+-binding, and a C-terminal dimerization domain (Figure 1.6). It has been shown that SCHAD forms homodimers, which are essential for its stability. The dimerization of two SCHAD molecules is mainly mediated by hydrophobic interactions between the C-terminal domains of each monomer [35].

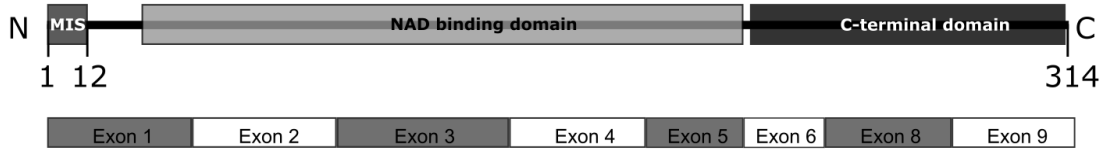

Figure 1.6 – Schematic organization of the domains of the SCHAD protein and coding exons. SCHAD has a total length of 314 amino acid residues. It has an N-terminal mitochondrial signal peptide (MIS), a NAD^+-binding domain and a C-terminal dimerization domain. The protein is encoded by 8 exons from the *HADH* gene, lacking exon number 7. Figure made based on gene ID 3033 and reference sequence NM_005327.4 in the NCBI database (https://www.ncbi.nlm.nih.gov/nuccore/NM_005327.4). Source: Kelly Velasco.

The N-terminal SCHAD domain consists of a β-α-β fold (eight stranded β-sheet flanked by α-helices), while the C-terminal domain is primarily α-helical (Figure 1.7) [35, 36]. The two domains are connected by a short highly conserved linker region [35]. In the context of the catalytic activity of SCHAD in the FAO pathway, the binding of the substrate takes place at the interface of the two domains. The active site contains a highly conserved histidine-glutamate pair [35], where the catalytic mechanism includes deprotonation of the substrate by the histidine residue, which works as a catalytic base. Then, the glutamate residue neutralizes the positive charge of the histidine. Presence of the NAD^+ cofactor greatly increases the affinity of the active site for the fatty acid oxidation substrate [37].

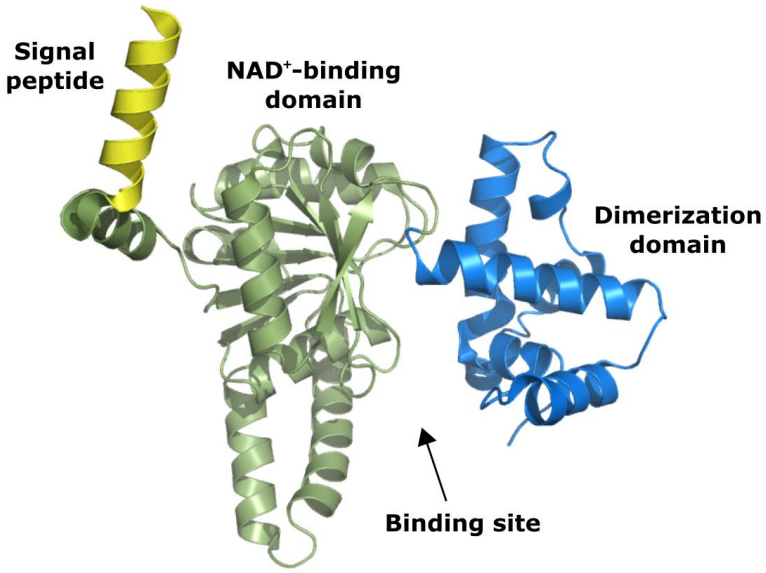

Figure 1.7 – Tri-dimensional model of SCHAD. SCHAD consists of mitochondrial signal peptide (yellow), a NAD^+ binding N-terminal domain (green) and a C-terminal dimerization domain (blue). The N-terminal domain contains a β-α-β-fold, while the C-terminal domain is primarily α-helical. The FAO substrate binds at the interface of the two domains. The image was obtained with the program PyMOL using the SCHAD molecular model 3RQS from the Protein Data Bank (PDB) (http://www.rcsb.org/structure/3RQS).

1.3.4 SCHAD functions

As already mentioned, SCHAD is considered to have two different roles: one in the FAO pathway and the second in the regulation of insulin secretion (Chapter 1.3.1). A number of studies suggest that these two SCHAD functions are independent off each other [33, 38] [34]. For instance, even though SCHAD is ubiquitously expressed in all cells, unlike the other FAO enzymes it has very high expression levels in the beta cells compared to the surrounding tissue [39]. The function of SCHAD in the FAO pathway will be briefly described below, while its role in insulin regulation will be discussed in Chapter 1.3.5.

Fatty acids are a source of energy during fasting, in addition to being a main source of energy for the heart, skeletal muscle and kidneys [40]. After being activated to acyl-coenzyme A (Co-A) in the cytosol, fatty acids are imported from the cytosol to the mitochondrial matrix by the carnitine shuttle where the FAO takes place. FAO is a cyclic process consisting of four steps (Figure 1.8), where each cycle releases two carbon atoms in the form of acetyl-CoA from the fatty acid that is degraded [40]. SCHAD catalyses the third of these steps, which is a dehydrogenation of 3-hydroxyacyl-CoA esters to 3-ketoacyl-CoA, coupled to the reduction of NAD^+ to NADH [41]. In each step of the cycle there are several overlapping chain length-specific enzymes; in the third step SCHAD is responsible for degrading fatty acids of short and medium length [36].

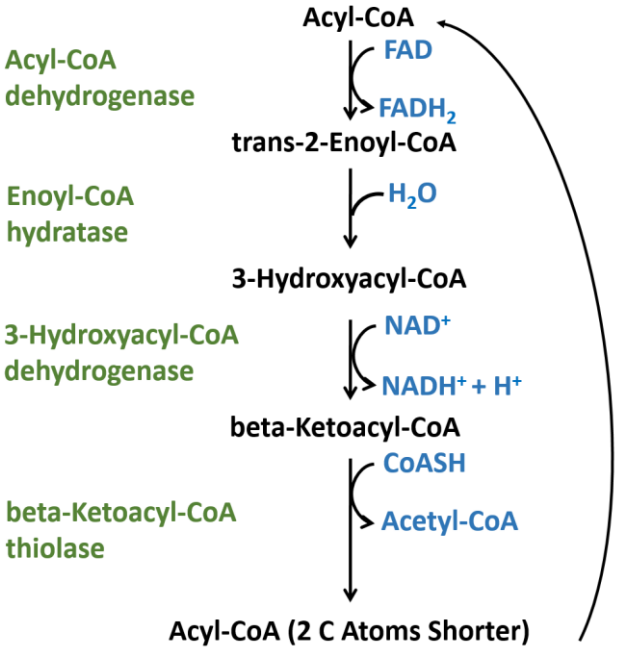

Figure 1.8 – SCHAD function in the FAO pathway. SCHAD catalyses the third of four enzymatic steps in the FAO, namely dehydrogenation of 3-hydroxyacyl-CoA esters to 3-ketoacyl-CoA, coupled to reduction of NAD^+ to NADH.

1.3.5 Mechanism of insulin dysregulation

It has been proposed that under normal conditions, SCHAD regulates the secretion of insulin through its interaction with GDH [38, 42]. GDH is, as described in Chapter 1.2.2.2, a mitochondrial enzyme that links the TCA cycle to the dehydrogenation of the amino acid glutamate, and thereby links carbohydrate and protein metabolism [43]. When bound to GDH, SCHAD inhibits GDH activity (Figure 1.9), which eventually will result in the down-regulation of insulin secretion from the beta cells. Thus, inactivating mutations in *HADH* would lead to a loss of the inhibitory protein interaction and an uncontrolled secretion of insulin [44].

Notably, the activating mutations in the GDH-encoding gene *GLUD1* also cause CHI (Chapter 1.2.2.2) [38]. CHI patients with mutations in either *GLUD1* or *HADH* are responsive to diazoxide treatment [29]. This is consistent with the fact that GDH lies upstream of the K_{ATP} channels in the pathway that triggers insulin secretion. Moreover, children with SCHAD CHI experience protein-induced hypoglycaemia [45], which might be explained by the role of leucine as an allosteric activator of GDH [46].

However, the mechanism by which SCHAD regulates insulin secretion and the downstream events are not completely understood. It was first suggested that the loss of inhibition on GDH by SCHAD results in increasing oxidation rates of glutamate to α-ketoglutarate (α-KG). α-KG enters the TCA cycle, increasing the production of ATP, and as a result insulin is released (Figure 1.9B) [38]. However, some experimental evidence indicates that – specifically in beta cells - GDH favours the opposite direction of this reversible reaction (e.g. glutamate formation) as a consequence of the beta cell NADH/NAD^+ ratio [47]. The produced glutamate would then be taken up by insulin secretory granules, which leads to amplification of insulin secretion (Figure 1.9A) [48-50].

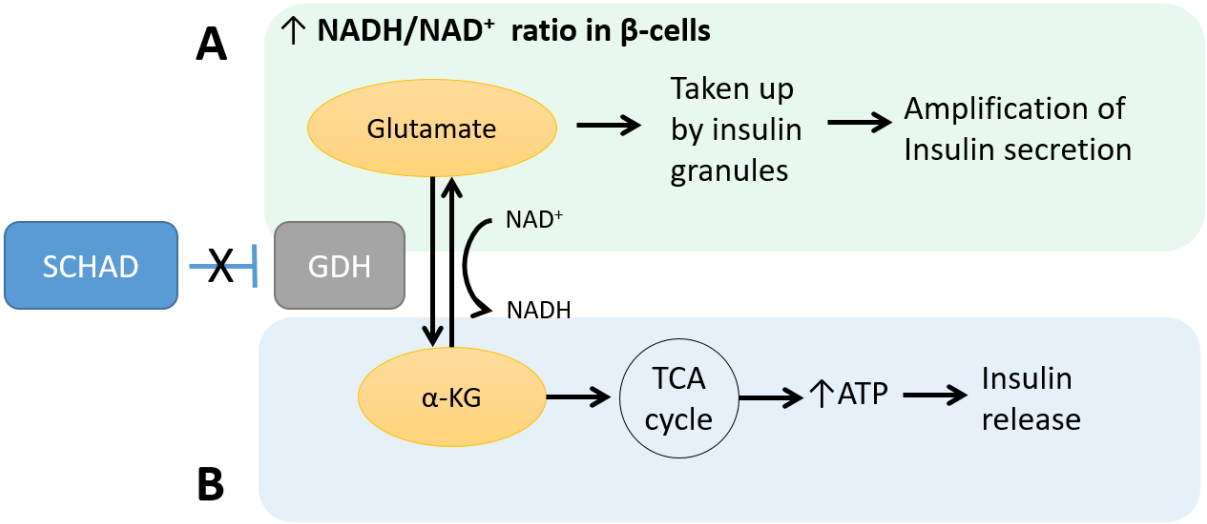

Figure 1.9 – Proposed mechanisms of insulin dysregulation in SCHAD deficiency. Under normal conditions SCHAD interacts with GDH and inhibits its enzymatic activity. **A**) GDH converts α-KG to glutamate, which is taken up by the secretory granules. The uptake of glutamate leads to amplification of the insulin secretion. The fate of α-KG depends on the ratio of NADH to NAD^+. **B**) Loss of inhibition of SCHAD on GDH result in a gain of GDH activity, which increases the oxidation of glutamate to α-KG. α-KG enters the TCA cycle, the production of ATP increases, and insulin is released.

In addition to the interaction with GDH, there is evidence of SCHAD could be involved in a large tissue-specific metabolic super complex where several metabolic pathways might converge [44]. The complex might involve several key regulatory enzymes from fatty acid oxidation, ketogenesis, amino acid catabolism, ureagenesis and glycolysis. This suggests that SCHAD might have additional organizational, structural and/or non-enzymatic roles, even outside of the mitochondria [44].

1.4 Classification of pathogenic variations in human genes

On average, the human genome has a variation in base sequence every few hundred bases. Variants can occur both in coding and non-coding areas. The 1000 Genomes project (http://www.internationalgenome.org) has estimated that an individual has 10000-11000 variants that change the amino acid sequence of proteins, and additional 10000-12000 exonic variants that have no effect. Approximately 50-100 variants per individual are associated with inherited disorders, but most individuals will only be carriers of the disease [51].

With the increasing use of whole-genome sequencing, variants are being discovered in the human genome at a high rate. This leads to a high demand to determine the clinical significance of a given variant. The American College of Medical Genetics and Genomics and the Association for Molecular Pathology have made a joint consensus for standards and guidelines for the interpretation of sequence variants. This includes a five-tier system of classification and can be used on all Mendelian genes. In the approach, criteria (evidence) of different strength are combined to determine the pathogenicity class of a variant (Table 1.2). Variants are then classified from 1-5 with the following designations: (1) pathogenic, (2) likely pathogenic, (3) uncertain significance, (4) likely benign, and (5) benign. The term "likely" means a greater than 90% certainty of a variant being either disease-causing or benign [52].

Table 1.2 - Criteria of different strength to determine pathogenicity. Criteria for benign to the left and pathogenic to the right. LOF = loss-of-function, MAF = minor allele frequency. Figure adapted from [52].

	Benign		Pathogenic			
	Strong	**Supporting**	**Supporting**	**Moderate**	**Strong**	**Very Strong**
Population data	MAF is too high for disorder or observation in controls inconsistent with disease penetrance			Absent in population database	Prevalence in affected persons statistically increased over controls	
Computational and predictive data		Multiple lines of computational evidence suggest no impact on gene / gene product Missense in gene where only truncating cause disease Splice variant with non predicted splice impact	Multiple lines of computational evidence support a deleterious effect on the gene / gene product	Novel missense change at an amino acid residue where a different pathogenic missense change has been seen before Protein length changing variant	Same amino acid change as an established pathogenic variant	Predicted null variant in a gene where LOF is a known mechanism of disease
Functional data	Well-established functional studies show no deleterious effect		Missense in gene with low rate of benign missense variants and pathogenic missenses common	Mutational hot spot or well-studied functional domain without benign variation	Well-established functional studies shown a deleterious effect	
Segregation data	Non-segregation with disease		Co-segregation with disease in multiple affected family members	Increased segregation data →		
De novo data				De novo (without paternity and maternity confirmed)	De novo (paternity and maternity confirmed)	
Allelic data		Observed in trans with a dominant variant Observed in cis with a pathogenic variant		For recessive disorders, detected in trans with a pathogenic variant		
Other databases		Reputable source without shared data = benign	Reputable source = pathogenic			
Other data		Found in case with an alternate cause	Patients phenotype or family history highly specific for gene			

1.4.1 Pathogenic variants of SCHAD

To date, there are 45 published patients with CHI caused by mutations in the *HADH* gene. Table 1.3 contains a list of the patients. All listed *HADH* mutations have an autosomal recessive inheritance. Dominantly acting mutations of this gene have not been seen.

Table 1.3 – Published patients with CHI caused by mutations in the HADH gene. The mutations are reported at the DNA level for splice site and intronic mutations, while the resulting effect on the protein is reported for those affecting the coding regions directly. NA = no information**.** Table adapted from [34].

Patient	Gender	Consanguinity	Ethnicity	Onset	Mutation	Reference
1	F	No	Indian	4 moths	P258L	[31]
2	M	Yes	Pakistani	3 days	IVS4-3DELCAGGTC	[32]
3	F	Yes	Pakistani	1.5 hours	IVS4-3DELCAGGTC	[32]
4	M	Yes	Pakistani	4 months	IVS6-2A>G	[53]
5	F	No	Caucasian	10 months	D57G, Y226H	[54]
6	F	Yes	Bangladeshi	4 months	M188V	[46]
7	M	Yes	Caucasian	2 months	R236X	[55]
8	M	Yes	Caucasian	8 months	S196FfsX3	[56]
9	F	Yes	Caucasian	6 months	S196FfsX3	[56]
10	M	NA	Caucasian	14 months	S196FfsX3	[56]
11	M	No	Caucasian	7 months	IVS2+1G>A	[56]
12	M	Yes	Turkish	16 weeks	K136E	[57]
13	M	Yes	Turkish	16 weeks	Q163X	[57]
14	M	Yes	Turkish	2 weeks	R236X	[57]
15	M	Yes	Turkish	5 days	R236X	[57]
16	F	No	Turkish	1 week	R236X	[57]
17	M	Yes	Pakistani	2 days	R236X	[57]
18	F	No	Iranian	12 weeks	R236X	[57]
19	F	No	Iranian	1 day	R236X	[57]
20	M	No	Indian	26 weeks	K95SfsX3, IVS6 + 39C>G	[57]
21	M	No	Indian	2 days	Ex1deletion	[57]
22	M	No	Indian	24 weeks	Ex1deletion	[57]
23	NA	NA	NA	NA	G34R	[30]

24	NA	NA	NA	NA	K95fs	[30]
25	NA	NA	NA	NA	IVS8+39C>G	[30]
26	F	NA	Chinese	NA	R10P, V30E	[58]
27	F	No	Indian	12 weeks	I184F	[16]
28	F	No	Indian	16 weeks	I184F	[16]
29	M	Yes	Saudi	16 weeks	IVS2-1G>A	[59]
30	F	Yes	Saudi	12 weeks	IVS2-1G>A	[59]
31	M	Yes	Saudi	16 weeks	IVS2-1G>A	[59]
32	F	No	Turkish	4 weeks	IVS2-1G>A	[60]
33	M	Yes	Iranian	12 weeks	IVS2-1G>A	[61]
34	F	Yes	Iranian	1 year	IVS2-1G>A	[61]
35	M	Yes	Iranian	1 day	IVS2-1G>A	[61]
36	F	Yes	Iranian	4 days	IVS2-1G>A	[61]
37	M	Yes	Iranian	12 weeks	IVS2-1G>A	[61]
38	M	Yes	Iranian	6 weeks	IVS2-1G>A	[61]
39	M	Yes	Iranian	30 weeks	IVS2-1G>A	[61]
40	F	Yes	Iranian	1 day	IVS2-1G>A	[61]
41	M	Yes	Iranian	12 weeks	IVS2-1G>A	[61]
42	M	Yes	Iranian	12 weeks	IVS2-1G>A	[61]
43	M	Yes	Iranian	12 weeks	IVS2-1G>A	[61]
44	M	No	Caucasian	NA	G303S	[62]
45	M	No	Indian	34 weeks	T189fs	[63]

2. Aims of the study

The overall objective of this thesis was to functionally characterize different rare variants of the SCHAD protein to obtain a better understanding of how this protein is involved in insulin secretion.

The specific sub-aims of the project were:

1. To express four rare SCHAD variants, reported as pathogenic, in bacterial and mammalian plasmid vectors
2. To evaluate the expression level, cellular localization, and enzymatic activity of the aforementioned four variants in vitro
3. To compare the protein stability of a series of rare SCHAD variants in human cells
4. To assess the interaction between a series of rare SCHAD variants and glutamate dehydrogenase
5. Based on the results, to make a formal classification of the degree of pathogenicity for SCHAD variants present in human populations

3. Materials

Table 3.1 – DNA techniques.

Material	Catalogue number	Supplier
1 kb DNA Ladder	N3232S	New England BioLabs
100 bp DNA Ladder	N3231S	New England BioLabs
2-propanol	I9516-500ML	Sigma Aldrich
Ampicillin sodium salt	A9518-5G	Sigma Aldrich
BL21 (DE3) competent E.coli cells	C2527I	New England Biolabs
CutSmart™ buffer	B7204S	New England BioLabs
D-(+)-Glucose powder	G7021	Sigma Aldrich
*Eco*RI-HF™	R3101S	New England BioLabs
Ethidium Bromide (10 mg/ml)	161-0433	Life Technologies
Gel Loading Dye Blue (6x)	B7021S	New England BioLabs
HisSpeed Plasmid midi kit	12643	Qiagen
ImMedia™ Amp Agar	45-0034	Invitrogen
ImMedia™ Kan Agar	45-0043	Invitrogen
Kanamycin Sulfate (100x)	15160-054	Life Technologies
LB broth (Lennox) growth medium	L7275-500TAB	Sigma Aldrich
NuSieve™ GTG™ Agarose	50084	Lonza
SOC Outgrowth medium	B9020S	New England Biolabs
TBE Buffer (10X)	A3945	PanReac AppliChem
XL 10-Gold Ultracompetent cells	200516-4	Agilent Technologies

Table 3.2 – Plasmids.

Plasmid	Description	Supplier
pcDNA3.1	Empty vector	Invitrogen
pcDNA3.1- SCHAD-V5	SCHAD-V5	Made by group
pET-MBP-SCHAD	MBP-SCHAD	Gift from Thomas Arnesen, University of Bergen
Plu-CMV-wt-hGDH-mCherry	Human GDH	Gift from Chonghong Li, University of Pennsylvania

Table 3.3 – Cell lines.

Cell line	Description	Catalogue number	Supplier
HEK293	Human embryonic kidney cells	632180	Clontech
HEK293 SCHAD KO	Human embryonic kidney cells with SCHAD knock out	-	Knock out done by Johanna Lüdeke (unpubl. data)

Table 3.4 – Reagents for cell culturing and transfection.

Material	Catalogue number	Supplier
Countess™ cell counting chamber slides	C10283	Invitrogen
Dimethyl sulfoxide (DMSO)	D2650-5X5ML	Sigma Aldrich
Dulbecco's Modified Eagle's Medium (DMEM)	41966-029	Gibco
Dulbecco's Phosphate Buffered Saline (PBS)	D8537	Sigma Aldrich
Fetal Bovine Serum (FBS)	10270-106	Gibco
OPTI-MEM® I (1X)	31985-062	Life Technologies
Penicillin-Streptomycin (PenStrep)	P4458	Sigma Aldrich
Trypan Blue stain 0.4%	T10282	Invitrogen
Trypsin-EDTA solution	T3924	Sigma Aldrich
HEPES	H2275-25G	Sigma Aldrich
$CaCl_2$	442909-1KG	Sigma Aldrich
Lipofectamine 2000 Transfection reagent	11668-019	Invitrogen

Table 3.5 – Antibodies.

Antibody	Catalogue number	Supplier	Dilution	Classification
Anti-β-Tubulin (rabbit)	Ab6046	Abcam	1:30000	Primary
Anti-GLUD1 (rabbit)	Ab166618	Abcam	1:1000	Primary
Anti-Mouse (goat)	626520	Invitrogen	1:5000	Secondary
Anti-Mouse Alexa Fluor 488 (goat)	Ab150113	Abcam	1:2000	Secondary
Anti-Rabbit (goat)	656120	Invitrogen	1:5000	Secondary
Anti-V5 (mouse)	R960-25	Invitrogen	1:15000	Primary

Table 3.6 – Site directed mutagenesis.

Material	Catalogue number	Supplier
*Dpn*I (10 U/µl)	200518-52	Agilent Technologies
QuickChange II XL Site-Directed Mutagenesis Kit	200522-5	Agilent Technologies
QuickChange XL dNTP Mix	200516-52	Agilent Technologies
TE buffer (pH 8)	Am9849	Ambicon

Table 3.7 – Sanger Sequencing.

Material	Catalogue number	Supplier
BigDye CTerminator® Purification kit	4376486	Thermo Fischer
BigDye® Terminator v1.1 Cycle Sequencing Kit	4337450	Thermo Fischer

Table 3.8 – Primers used for PCR amplification and Sanger Sequencing.

Primer	Direction	Sequence (5' to 3')
G34A	Forward	CAGCCCGCCGCGGATGACCGTCA
G34A_as	Reverse	TGACGGTCATCCGCGGCGGGCTG
HADH seq 3	Forward	CAGACAAGACCGATTCGCT
HADH seq 6	Reverse	CGATGACCGTCACGTGCTT
HADH seq 8	Forward	GAGAAGACCCTGAGCACCAT
HADH seq10	Reverse	GGATGTCCTCTGTCTGGTCT
HADH seq11	Reverse	CCAGGAGGCGGTTCACAATA
HADH-V5	Forward	AGGCTGTATGAACGAGGTGA
HADH-V5	Reverse	GGAGAGGGTTAGGGATAGGC
I184F	Forward	CTGGTCATTGGTGTTTTAAAGACCTCCACAAGTTTCATG
I184F_as	Reverse	CATGAAACTTGTGGAGGTCTTTAAAACACCAATGACCAG
K136E	Forward	TATGTTCAGCAGCAAACTCGTCCAGCCTTTTGAAGAG
K136E_as	Reverse	CTCTTCAAAAGGCTGGACGAGTTTGCTGCTGAACATA
M188V	Forward	CTTCTGGCTGGTCACTGGTGTTTTAATGACCTCC
M188V_as	Reverse	GGAGGTCATTAAAACACCAGTGACCAGCCAGAAG
pcDNA_HADHpl_FW	Forward	GCACCAAAATCAACGGGACT
pcDNA_HADHpl_RV	Reverse	TTGTCTTCCCAATCCTCCCC
β-actin	Forward	CTGGGACGACATGGAGAAAA
β-actin	Reverse	AAGGAAGGCTGGAAGAGTGC

Table 3.9 – Cell lysis, SDS-PAGE and Western Blotting.

Material	Catalogue number	Supplier
Blotting-Grade Blocker nonfat dry milk	170-6404	Bio-Rad
c0mplete Tablets, Mini EASYpack	04693124001	Sigma Aldrich
ECL Select™ Western Blotting Detection Reagent	RPN2235	GE Healthcare
ECL™ Primer Western Blotting Detection Reagent	RPN2232	GE Healthcare
Immun-Blot® PVDF Membranes for Protein Blotting	1620177	Bio-Rad
Methanol	A456-212	Thermo Fisher Scientific
NuPAGE® Antioxidant	NP0005	Thermo Fisher Scientific
NuPAGE® LDS Sample Buffer (4x)	NP0007	Thermo Fisher Scientific
NuPAGE® MOPS SDS Running Buffer (20x)	NP0001	Thermo Fisher Scientific
NuPAGE® Reducing Agent (10x)	NP0009	Thermo Fisher Scientific
NuPAGE® Transfer Buffer (20x)	NP0006-1	Thermo Fisher Scientific
NuPAGE™ 10% Bis-Tris Gel 1.0 mm x 10 well	NP0301BOX	Thermo Fisher Scientific
NuPAGE™ 10% Bis-Tris Gel 1.0 mm x 15 well	NP0303BOX	Thermo Fisher Scientific
Phosphate Buffer saline (PBS) Tablets	18912-014	Life Technologies
Pierce® RIPA Buffer, 100 ml	89900	Thermo Scientific
Pierce™ BCA Protein Assay Kit	23227	Thermo Scientific
Precision Plus ProteinTM Standards All Blue	161-0373	Bio-Rad
Restore™ PLUS Western Blot Stripping Buffer	46430	Thermo Scientific
SimplyBlue™ Safestain	LC6065	Life Technologies
Tween ®	P5927	Sigma Aldrich
Western Blotting Filter Paper, 7cm x 8.4cm	84783	Thermo Scientific
XCell SureLock™ Mini-Cell and XCell II™ Blot Module	EI0002	Thermo Fisher Scientific

Table 3.10 – Immunofluorescence.

Material	Catalogue number	Supplier
Bovine Serum Albumin (BSA)	A7030-50G	Sigma Aldrich
Cover slips (18 mm)	117580	Werderop Werd
Ethanol pure	20821	VWE
Formaldehyde solution	252549-IL	Sigma-Aldrich
Glycine	50052-1KG	Fluka Analytical
MitoTracker® Red CMXRos	M7512	Thermo Fisher lb
Mounting glass	2009-08	Thermo Scientific
Poly-L-lysine	P4832-50ml	Sigma Aldrich
ProLong® Gold antifade reagent with DAPI	P36935	Life Technologies
Triton™ X-100	T8787	Sigma Aldrich

Table 3.11 – TNT assay.

Material	Catalogue number	Supplier
TNT® Quick Coupled Transcription/Translation System	L1170	Promega

Table 3.12 – Reverse Transcriptase PCR.

Material	Catalogue number	Supplier
dNTP Mixture	4030	TaKaRa Clonetech
High Capacity cDNA Reverse Transcription Kit	4374966	Applied Biosystems™
LA Taq® DNA Polymerase with GC Buffer	RR02AG	TaKaRa Clonetech
RNeasy® Mini Kit (250)	74106	Qiagen

Table 3.13 – Protein purification and enzymatic assay

Material	Catalogue number	Supplier
Acetoacetyl-CoA	A1625-5MG	Sigma Aldrich
DTT	43816-10ML	Sigma Aldrich
Glycerol	G2025-1L	Sigma Aldrich
HiLoad 16/60 Superdex 200 prep grade	28989335	GE Healthcare Life Sciences
HisTrapHP	17-5248-01	GE Healthcare Life Sciences
Imidazole	AC122020020	ACROS Organics
IPTG	I6758	Sigma Aldrich
K_2HPO_4	105101	Merck
KH_2PO_4	104873	Merck
MES hydrate	M5287-250G	Sigma Aldrich
NaCl	793566-2.5KG	Sigma Aldrich
NADH	N1161-10V	Sigma Aldrich
NaH_2PO_4	71507	Sigma Aldrich
NaOH	0402	J.T. Baker
Peptone	70172-500G	Fluka Analytical
Protease inhibitors cOmplete, EDTA free	11873580001	Roche
Yeast extract	103753	Merck

Table 3.14 - Cycloheximide chase assay

Material	Catalogue number	Supplier
Cycloheximide	C4859 (1 ml)	Sigma Aldrich

Table 3.15 - Co-immunoprecipitation assay.

Material	Catalogue number	Supplier
Pierce® Co-Immunoprecpitation Kit	26149	Thermo Scientific

Table 3.16 – Buffers and solutions.

Buffers and solutions	Use	Composition
10% Transfer buffer	Western Blotting	50 mL NuPAGE® MOPS transfer buffer (20x), 1 ml NuPAGE® Antioxidant, 100 ml methanol, 849 ml deionized water
2x HBS buffer, pH 7	Transfection	50 mM HEPES, 280 mM NaCl, 1.5 mM Na_2HPO_4, dissolved in Mq H_2O, pH 7
Blocking buffer	Immunofluorescence	5 ml 4% BSA solution, 4.5 ml 100 mg/ml glycine solution, 10.5 ml PBS-Tween
Elution buffer	Protein purification	50 mM NaH_2PO_4, 300 mM NaCl, 250 mM Imidazole, 10% glycerol, 0.1 mM DTT, ddH_2O to total volume 80 ml, pH 7.9
Enzymatic assay buffer	Enzymatic assays	0.1 M potassium phosphate buffer pH 7.0, 0.1 mM DTT, 0.3 mg/ml BSA, 50 µM Acetoacetyl-CoA, 0.15 mM NADH
Gel filtration buffer	Protein purification	50 mM NaH_2PO_4, 150 mM NaCl, 10% glycerol,0.1 mM DTT, ddH2O to total volume of 500 ml, pH 7.9
Lysis buffer	Protein purification	50 mM NaH_2PO_4, 500 mM NaCl, 10 mM Imidazole, 10% glycerol, 0.1 mM DTT, ddH_2O to total volume 100 ml, pH 7.9
PBS-Tween (0.1%)	Immunofluorescence, Western Blotting	PBS tablets and 10% Tween dissolved in mqH2O
Permeabilization buffer	Immunofluorescence	0.4 ml 10% Triton-X-100, PBS to 20 ml
Washing buffer	Protein purification	50 mM NaH_2PO_4, 300 mM NaCl, 20 mM Imidazole, 10% glycerol, 0.1 mM DTT, ddH_2O to total volume 150 ml, pH 7.9
Potassium phosphate buffer	Enzymatic assay	15.38 ml K_2HPO_4, 7.7 ml KH_2PO_4, adjust to pH 7.0 with NaOH, ddH_2O to total volume 250 mL

Table 3.17 - Technical equipment.

Instrument	Manufacturer
Applied Biosystems 3500xL Genetic Analyzer	Thermo Fischer
BioTek™ ELx808™ Absorbance Microplate Reader	Fischer Scientific
Countess™ Automated Cell Counter	Invitrogen
Eclipse E800 Microscope	Nikon
GBOX I Chemi XR5	Syngene
GeneAmp® PCR System 2700	Applied Biosystems
GeneFlash ABI 3500xl	Syngene
Leica Confocal SP5	Leica Microsystems
MBA 2000 UV/VIS Spectrophotometer	Perkin Elmer
NanoDrop ND-1000 Spectrophotometer	Thermo Fischer Scientific
UV-visible Spectroscopy System 8453	Agilent

Table 3.18 - Analytical Software.

Software	Supplier
Alamut® Visual	Interactive Biosoftware
GIMP 2 (GNU Image Manipulation Program)	GIMP
Image Studio™ Lite	LI-COR®
InkScape 0.92.2	InkScape
Leica Application Suite X (LAS X)	Leica Microsystems
PyMOL	Schrödinger
QuickChange Primer Design	Agilent
SnapGene Viewer	SnapGene

4. Methods

4.1 Construction of four new SCHAD variants

4.1.1 Primer design

Primers needed for the construction of four new SCHAD variants (Table 4.1) were designed using the web-based QuickChange Primer Design Program from Agilent (https://www.genomics.agilent.com/primerDesignProgram.jsp). Primers were dissolved in TE buffer to a 100 μM concentration and stored at -20˚C.

Table 4.1 – Sequences of primers used to construct the four SCHAD variants G34R, K136E, I1844F and M188V.

Primer	Sequence (5' to 3')
G34R	CAGCCCGCCGCGGATGACCGTCA
G34R_as	TGACGGTCATCCGCGGCGGGCTG
K136E	TATGTTCAGCAGCAAACTCGTCCAGCCTTTTGAAGAG
K136E_as	CTCTTCAAAAGGCTGGACGAGTTTGCTGCTGAACATA
I184F	CTGGTCATTGGTGTTTTAAAGACCTCCACAAGTTTCATG
I184F_as	CATGAAACTTGTGGAGGTCTTTAAAACACCAATGACCAG
M188V	CTTCTGGCTGGTCACTGGTGTTTTAATGACCTCC
M188V	GGAGGTCATTAAAACACCAGTGACCAGCCAGAAG

4.1.2 Site-directed mutagenesis

The four missense mutations were introduced in the mammalian pcDNA3.1-SCHAD-V5 (Figure 4.1A) and the bacterial pET-MBP-SCHAD (Figure 4.1B) expression vectors by the use of the QuickChange II XL Site-Directed Mutagenesis Kit from Agilent Technologies.

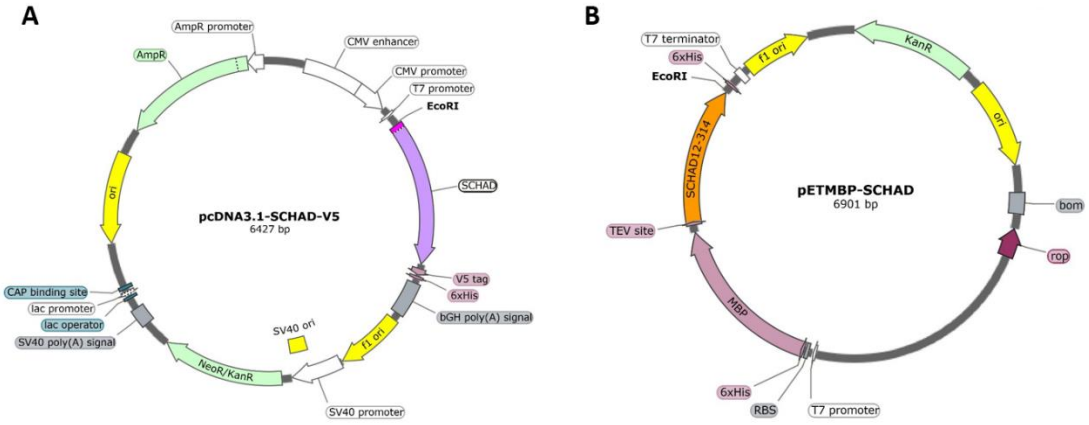

Figure 4.1 – Plasmid maps. A) pcDNA3.1-SCHAD-V5**. B)** pET-MBP-SCHAD.

The reaction mixes for the mutagenesis reactions were prepared as shown in Table 4.2, and PCR amplifications were run as shown in Table 4.3.

Table 4.2 – Master mix components for site directed mutagenesis.

Component	Volume
10 x reaction buffer	5.0 µl
DNA template	10.0 ng
Reverse primer (10 µM)	1.25 µl
Forward primer (10 µM)	1.25 µl
dNTP mix	1.0 µl
QuickSolution reagent	3.0 µl
*Pfu*Ultra High Fidelity DNA Polymerase	1.0 µl
MQ H_2O	To final volume of 50.0 µl

Table 4.3 – Amplification conditions for site-directed mutagenesis.

Step	Temperature (˚C)	Duration	Cycles
Pre-denaturation	95	1 min	1
Denaturation	95	50 sec	18
Annealing	60	50 sec	
Elongation	68	1 minute / kb plasmid length: SCHAD-V5 = 6 min 24 sec MBP-SCHAD = 6 min 54 sec	
Final elongation	68	7 min	1
Cooling	4	∞	

To digest parental methylated and hemimethylated dsDNA, 1 µl *Dnp*I restriction enzyme (10 U/µl) was added to each amplification reaction. The samples were incubated at 37˚C for 1 hour.

4.1.3 Transformation of XL10-Gold Ultracompetent Cells

The *Dpn*I-treated reactions were used for transformation into XL10-Gold Ultracompenent cells by the heat shock method. Two µl β-mercaptoethanol was added to 45 µl bacteria cells and incubated on ice for 10 minutes. Two µl of *Dpn*I-treated DNA was added to the cells, followed by incubation on ice for 30 minutes. Cells were heat-shocked at 42˚C for 30 seconds, and after 2 minutes of incubation on ice, 0.5 ml preheated SOC medium was added to the tube. Cells were incubated for 1 hour at 37˚C on vigorous shaking (250 rpm), before plating 80 µl of the transformation reaction on selective agar plates (MBP-SCHAD = kanamycin, V5-SCHAD = ampicillin). After approximately 16 hours, 2 ml selective LB medium was inoculated by one bacteria colony. The starter culture was incubated for 8 hours at 37˚C with vigorous shaking

(250-300 rpm) before diluting it 1/1000 in 50 ml selective LB medium. The culture was grown overnight and harvested by centrifugation at 4000 g for 20 minutes. The supernatant was removed and the pellet was frozen at -20˚C until further use. Plasmid purification was performed as described in Chapter 4.2.1.

4.1.4 Sanger Sequencing

After preparation, all plasmids were verified by Sanger sequencing by the use of the BigDye Terminator v.1.1 Cycle Sequencing Kit. Sequencing mixes were made as shown in Table 4.4. Separate mixes were made for each of the primers. Their target sequences are shown in Table 4.5. The thermal amplification program is presented in Table 4.6.

Table 4.4 – Components for Sanger sequencing.

Reagents	Volume
BigDye Terminator v.1.1 Ready Reaction mix	1.0 µl
BigDye Terminator v.1.1 5x Sequencing Buffer	2.0 µl
Sequencing primer (2 µM)	1.0 µl
Plasmid	2.0 µl
MQ H2O	4.0 µl
Final volume	10.0 µl

Table 4.5 – Primers used for sequencing of SCHAD variants.

Primer	DNA target sequence (5’ to 3’)
HADH Seq 3	CAGACAAGACCGATTCGCT
HADH Seq 6	CGATGACCGTCACGTGCTT
HADH Seq 8	GAGAAGACCCTGAGCACCAT
HADH Seq 10	GGATGTCCTCTGTCTGGTCT
HADH Seq 11	CCAGGAGGCGGTTCACAATA
pcDNA_HADHpl_FW	GCACCAAAATCAACGGGACT
pcDNA_HADHpl_RV	TTGTCTTCCCAATCCTCCCC

Table 4.6 - Thermal amplification cycles for Sanger sequencing.

Step	Temperature	Duration	Cycles
Pre-denaturation	96˚C	1 min	1
Denaturation	96˚C	10 sec	25 cycles
Annealing	50 ˚C	5 sec	
Elongation	60˚C	4 min	
Cooling	4˚C	∞	

After the PCR amplification, 15 µl MQ H_2O was added to each reaction before proceeding to PCR purification by the use of a Bigdye XTerminator Kit. Forty-five µl SAM solution and 10 µl BigDye XTerminator bead solution were added to 10 µl of the amplified sample in a 96-well sequencing plate. A MicroAmp Clear Adhesive Film was used to seal the samples, and the plate was shaken at 1800 rpm for 20 minutes. The reactions were then centrifuged for 2 minutes at 1000 g, and placed in a capillary electrophoresis instrument used for sequencing (GeneFlash ABI 3500xl). Sequences were analysed using the sequencing analysis program SnapGene.

4.2 Plasmid purification and evaluation of DNA quality

4.2.1 Plasmid purification

Plasmids were purified from a 50 ml overnight culture by the use of a HiSpeed Plasmid Midi Kit. The purification was performed as described in the manufacturer's handbook (May, 2012). In short, pelleted bacterial cells were resuspended in resuspension buffer (with RNase A), and lysed in alkaline lysis buffer (with NaOH and SDS). After addition of neutralization buffer, precipitates were cleared from the lysate by filtrating through a QIAfilter Cartridge. Plasmid DNA was then filtered from the lysate by a HiSpeed Tip by gravity flow. After washing, the plasmid DNA was eluted in a high-salt buffer and concentrated by isopropanol precipitation. A QIAprecipitator Module was used to collect the DNA, and the DNA was eluted with 1 ml buffer TE.

4.2.2 OD measurements

The concentration and purity of the plasmid DNA preparations were measured by the use of NanoDrop ND-1000 spectrophotometer. The concentration in a sample was determined as the average of three measurements. A preparation with a 260/280 nm absorbance ratio around 1.8 to 2.0 was considered of sufficient purity.

4.2.3 Agarose gel electrophoresis

To further evaluate the quality of the plasmid preparation, untreated samples and samples treated with a restriction enzyme were subjected to electrophoresis in a 1% agarose gel containing 0.5 µg/ml ethidium bromide. Restriction digestion with *Eco*RI, which has a unique cutting site in the plasmids, was used to confirm that they had the expected size. Samples were prepared as shown in Table 4.7. The cut plasmid reactions were incubated at 37˚C for 15 minutes before adding the loading buffer.

Table 4.7 – Sample preparation for restriction digestion and agarose gel electrophoresis.

Component	Cut plasmid	Uncut plasmid
Plasmid	250.0 ng	100.0 ng
10x Cutsmart buffer	5.0 µl	-
*Eco*R1	1.0 µl	-
6x Loading dye	10.0 µl	1.0 µl
MQ H_2O	To final volume of 50.0 µl	To final volume of 6.0 µl

Samples were run adjacent to a 1 kb DNA ladder to estimate the size of the fragments. The gel was run at 90V for 1-2 hours in 1x TBE buffer.

4.3 Cell culture and transfection

4.3.1 Culturing

Human Embryonic Kidney cells (HEK293) were cultured in DMEM supplemented with 10% FBS and 1% Penicillin Streptomycin (Pen Strep). The cells were incubated in humidified air at 37˚C with 5% CO_2. All work was done in a sterile hood. Standard HEK293 cells and HEK293 SCHAD KO cells were cultured under the same conditions.

4.3.2 Culture maintenance and sub-culturing

Cells were split twice a week when the confluency was 80-90%, and in addition the medium was changed once in between. Cells were grown in either T75 or T25 flasks. Upon splitting, cells were washed in PBS and detached from the flask with 0.05% Trypsin-EDTA solution (T75 = 5 ml, T25 = 1 ml). After a 5-minute incubation period, fresh medium (T75 = 7 ml, T25 = 4 ml) was added to the cells and a homogenous cell suspension was made by pipetting. Cells were diluted 1/10 in fresh medium (total volume T75 = 10 ml and T25 = 5 ml) and seeded again. The remaining cells were used in experiments or discarded.

4.3.3 Cell counting

After trypsinization, cells were counted in a Countess automated cell counter machine. To be able to estimate cell viability, 15 µl of the cell suspension was mixed with equal amounts of Trypan Blue. Ten µl of the mix was added to each of two separate chambers in a counting cell which was then inserted in the machine to proceed with the quantification. The average value of viable cells for both chambers was calculated and used as the cell number.

4.3.4 Freezing and thawing

For freezing, cells from one T75 flask were trypsinized and resuspended in 5 ml complete medium. The cells were spun down at 200 g for 5 minutes and the supernatant was removed. The pellet was then re-suspended in 3 ml freezing medium (10% (v/v) DMSO in complete medium). This cell suspension was then divided in 1 ml aliquots in cryo-vials and placed in a Coolcell. The Coolcell was kept at -80˚C overnight, before transferring the vials to liquid nitrogen for long term storage.

To start a new culture, a vial was removed from liquid nitrogen and the cell suspension was rapidly thawed by hand-warming, before transferring the content to a tube containing 9 ml complete growth medium. Cells were spun down for 5 minutes at 125 g before removing the supernatant. The pellet was resuspended in 10 ml complete media and the whole volume was transferred to a T75 flask.

4.3.5 Transient transfection of HEK293 cells

4.3.5.1 Transfection by the calcium phosphate method

Transfection of plasmids to HEK293 cells grown in 10 cm petri dishes was done by the calcium phosphate method. Two solutions, A and B, were prepared in separate tubes as shown in Table 4.8. Solution B was added dropwise to solution A while vortexing, and the mix was incubated at RT for 5 minutes. The solution was then added drop-wise directly to the medium of the cells and evenly distributed in the plate. After 4 hours of incubation at 37˚C with 5% CO_2 the transfection medium was replaced with 10 ml fresh medium. The cells were harvested approximately 48 hours after transfection.

Table 4.8 – Components for transfection by the calcium phosphate method.

Solution	Component	Volume
A	2x HBS	600.0 µl
B	Plasmid	10.0 µg
	$CaCl_2$	72.3 µl
	MQ H_2O	To final volume of 600.0 µl

4.3.5.2 Transfection using Lipofectamine

Cells grown in 6- and 12-well plates were transfected by the Lipofectamine method at a confluency of 60-70%. OptiMEM (12-well = 50 µl, 6-well = 100 µl) was added to two 1.5 ml tubes. DNA (12-well = 1 µg, 6-well = 4 µg) was added to one of the tubes, while Lipofectamine (12-well = 4 µl, 6-well = 10 µl) was added to the other. The DNA mixture was then added to

the Lipofectamine mixture and incubated at RT for 5 minutes, before equally distributing the solution directly in the medium of the cells. After 4 hours the medium was exchanged by fresh medium.

4.4 SDS-PAGE and western blotting

4.4.1 SDS-PAGE

In general, samples for SDS-PAGE were prepared with a protein concentration ranging from 1-5 µg in a total volume of 10-20 µl with 1x loading buffer and reducing agent. Samples were denatured on a heating block at 70-90˚C for 10-20 minutes. For separation by gel electrophoresis, samples were loaded in 10% NuPage Bis-Tris gels adjacent to 3 µl Precision Plus Protein standard. Five-hundred µl NuPAGE Antioxidant were added to the running buffer in the inner buffer chamber of the XCell SureLock Mini-cell. Gels were run in 1x MOPS NuPAGE SDS running buffer for approximately 75 minutes at 160V.

4.4.2 Coomassie staining

Gels were stained using SimplyBlue SafeStain according to the manufacturers microwave procedure (February, 2012). After electrophoresis, the gel was placed in approximately 100 mL ddH_2O and microwaved until the solution almost boiled. The gel was shaken on an orbital shaker for 1 minutes before discarding the water and repeating the above steps two times. Approximately 20 ml SimplyBlue SafeStain was then added to the gel. After microwaving for 45 seconds, the gel was incubated in the solution at shaking for 5 minutes. Finally, the gel was washed in ddH_2O for 10 minutes, and imaged on a GBOX I Chemi XR5 instrument.

4.4.3 Western blotting

Proteins were transferred to a polyvinylidene fluorid (PVDF) membrane (pre-activated in methanol) in NuPage transfer buffer for 70 minutes at 30 V according to the manufacturer's instructions using the XCell II Blot Module. Following transfer, membranes were blocked in 3% dry milk diluted in PBS-Tween for 1 hour at RT. Antibodies were diluted in the same solution. Primary antibodies were incubated for 1 hour at RT or overnight at 4˚C, and secondary horseradish peroxidase (HRP) conjugated antibodies for 1 hour at RT. The membrane was washed in PBS-Tween after each antibody incubation (4 x 15 min). Amersham ECL Prime or Select Western Blotting Detection Reagent were used as substrate for HRP activity from the bound secondary antibodies, and the produced signal was imaged on a GBOX I Chemi XR5 instrument.

4.5 SCHAD-V5 protein expression level assessment by western blotting

Protein expression of SCHAD-V5 was tested in both standard HEK293 cells and HEK293 SCHAD KO cells. $1.0x10^5$ cells were seeded per well in a 12-well plate, and after 24 hours, the cells were transfected with the Lipofectamine reagent (4.3.5.2).

4.5.1 Lysis of HEK293 cells for protein extraction

Forty-eight hours post transfection cells were washed twice in PBS and lysed in 100 µl/well cold RIPA buffer with 1x protease inhibitor for five minutes. Cells were transferred to 1.5 ml tubes and centrifuged at 14000 g for 15 min at 4˚C. The pellet was then discarded, and the protein concentration of the supernatant measured by the use of a Bicinchoninic Acid (BCA) assay.

4.5.2 Protein concentration determination

Protein concentration of the cell lysate was measured by the use of a BCA protein assay kit following the manufacturer's instructions. Bovine serum albumin (BSA) standards with a concentration ranging from 0.0-2.5 mg/ml were used to make a standard curve. The unknown concentrations were determined by interpolation of the graph.

4.6 Cell-free protein expression

The expression of SCHAD-V5 variants was tested using the TNT Coupled Transcription/Translation system, which provides all the needed components to produce eukaryotic proteins from vectors containing a T7 promoter in a cell-free environment. The reaction components were assembled as described in Table 4.9 and incubated at 30˚C for 60 minutes. Protein synthesis was assessed by western blotting. Samples were prepared as shown in Table 4.10, and SCHAD-V5 was detected by anti-V5.

Table 4.9 – Components of the TNT assay.

Components	Volume
TNT Quick Master Mix	20.0 µl
Methionine, 1 mM	0.5 µl
Plasmid DNA template	0.5 µg
Nuclease-free water	To final volume of 25.0 µl

Table 4.10 – TNT sample preparation for western blotting.

Components	Volume
Reaction sample	3.0 µl
4x Loading buffer	2.5 µl
10x Reducing agent	1.0 µl
MQ H_2O	3.5 µl
Final volume	10.0 µl

4.7 Reverse transcriptase PCR of SCHAD variants

HEK293 SCHAD KO cells ($2.5x10^5$) were seeded in a 6-well plate. After 24 hours, the cells were transfected with Lipofectamine (Chapter 4.3.5.2). Forty-eight hours after transfection the medium was removed and the cells were washed with PBS. Cells were detached with 1 ml Trypsin-EDTA and resuspended in 2 ml fresh medium after incubation. The content of each well was transferred to separate tubes and centrifuged at 300 g for 5 minutes. The supernatant was discarded and the pellet resuspended in PBS. Cell concentrations were determined (Chapter 4.3.3) to find the volume needed to make aliquots containing $5x10^5$ cells per tube. Once aliquoted, cells were pelleted by centrifugation for 5 minutes at 300 g. Supernatants were discarded, while the pellets were stored at -80˚C until further use.

RNA was purified from the cell pellets using a RNeasy Micro Kit as described in the manufacturer's handbook (December, 2014). In short, cells were lysed with a guanidine thiocyanate buffer (buffer RLT) and homogenized by vortexing. 70% ethanol was added to enhance the subsequent binding of nucleic acids to a silica membrane. The sample was then added to a spin column containing the silica membrane and the DNA was digested by DNase (in buffer RDD). After washing, total RNA was eluted in 30 µl RNase-free water. The concentration and quality of the RNA samples were measured with a NanoDrop spectrophotometer, and samples were stored at -20˚C until further use.

The purified RNA was used to synthesize single-stranded cDNA using the High-Capacity cDNA Reverse Transcription Kit. A master mix was prepared as shown in Table 4.11. Four-hundred µg RNA was added to 10 µl of the master mix in equal volume. The samples were then centrifuged for 1 minute at 1000 rpm and incubated at 25˚C for 10 minutes, 37 ˚C for 120 minutes and 85 ˚C for 5 minutes followed by cooling at 4˚C.

Table 4.11 – Components for cDNA reverse transcription.

Component	Volume/reaction
10x RT buffer	2.0 µl
25x dNTP mix (100 mM)	0.8 µl
10x RT Random Primers	2.0 µl
MµltiScribe Reverse Transcriptase	1.0 µl
Nuclease-free H2O	4.2 µl
Final volume	10.0 µl

The synthesized cDNA was used as a template to amplify the specific products from the HADH-V5 constructs by PCR. Actin primers were used as positive and loading controls (see list of primers Table 3.8). A PCR master mix was prepared as described in Table 4.12. Two µl cDNA template was added to 18 µl of the master mix, and PCR amplification was run as described in Table 4.13.

Table 4.12 – Master mix components for cDNA PCR.

Component	Volume
2xGC buffer	10.0 µl
dNTP mix (2.5 mM)	3.2 µl
HADH-V5 (F) primer (20 µM)	0.4 µl
HADH-V5 (R) primer (20 µM)	0.4 µl
B-Actin (F) primer (20 µM)	0.4 µl
B-Actin (R) primer (20µM)	0.4 µl
ddH_2O	3.4 µl
LaTaq enzyme (5U/µl)	0.2 µl
Final volume	18.4 µl

Table 4.13 – Thermal amplification for cDNA PCR.

Step	Temperature (˚C)	Time	Cycles
Pre-denaturation	94	1 min	1
Denaturation	94	30 sec	
Annealing	59	30 sec	25
Elongation	72	1 min 30 sec	
Final elongation	72	10 min	1
Cooling	4	∞	

For analysis, the PCR products were run on a 2% agarose gel. Six µl of the PCR products were mixed with 3 µl 6x loading buffer and loaded in the wells. A 100 bp DNA ladder was used as a marker. The gel was run at 90V for 60 minutes.

4.8 Assessment of protein expression and subcellular localization by immunofluorescence

Expression and subcellular localization of the SCHAD-V5 variants were tested by immunofluorescence. Before cell seeding, a coverslip was placed in each well of a 12-well plate. The coverslips had been previously cleaned and sterilised by washing in ethanol and flamed. One ml of poly-L-lysine diluted 1/10 in PBS was added to each well and incubated for 5 minutes. The slides were then washed twice in PBS and allowed to dry. $1.0x10^5$ HEK292 SCHAD KO cells were seeded per well. After 24 hours, the appropriate plasmid was transfected with Lipofectamine (Chapter 4.3.5.2). After a 48 hours growth period, cells in each well were incubated with 1 ml 200 mM Mito Tracker prepared in pre-warmed media for 30 minutes. After washing with PBS, cells were fixated by incubation in 1 ml 3.7% paraformaldehyde with complete media for 15 minutes and then washed three times in PBS. Cells were permeabilized with 500 µl 0.2% Triton X-100 in PBS for 10 minutes under gentle shaking. After 3 x 5 minutes washing in PBS, 500 µl blocking buffer was added to each well for 30 minutes under gentle shaking. The cells were incubated with primary (anti-V5, 1:500) and secondary (anti-mouse Alexa Fluor 488, 1:200) antibodies diluted in PBS in a humidified chamber, each for 1 hour at room temperature. The cells were washed 3 x 5 minutes in PBS after the antibodies incubations. Finally, coverslips were mounted on a small drop of ProLongGold mounting medium with DAPI placed on clean glass slides. Images of the cells were taken using a Nicon Eclipse E800 fluorescence microscope and a Leica Confocal SP5 microscope.

4.9 Cycloheximide chase assay

3.0×10^5 HEK293 SCHAD KO cells were seeded per well in a 12-well plate. Four wells were transfected in parallel per SCHAD-V5 variant (for harvesting at four different time points) with Lipofectamine (Chapter 4.3.5.2). Forty-eight hours post transfection, the medium was removed and fresh medium with 50 µg/ml cycloheximide was added. Cells were harvested after 0, 2, 8 and 24 hours. For each time point, the cells were washed twice in ice cold PBS and lysed as described in Chapter 4.5.1. The cell lysates were frozen straight after harvesting and the centrifugation was performed for all samples in parallel >24 h post freezing. The protein concentration of the cell lysate was measured using the BCA kit (Chapter 4.5.2) and the samples were analysed by western blotting as explained in Chapter 4.4.3.

4.10 Protein purification and enzymatic assays of MBP-SCHAD

4.10.1 Transformation of BL21 competent *E. coli* cells

Transformation of MBP-SCHAD to competent BL21 (DE3) *E .coli* cells was done by heat shock. A tube of cells was thawed on ice until the last ice crystals disappeared. Around 10 ng plasmid DNA was added to the cells bfore the cell mixture was placed on ice for 30 minutes. Cells were then heat-shocked at 42 ˚C for 10 seconds and placed on ice for 5 minutes. SOC medium (950 µl) at RT was added to the tube, and the mixture was shaken vigorously at 700 rpm for 60 minutes. Forty µl of cells were spread on previously prepared imMedia Growth Medium agar plates (50 µg/ml kanamycin) and incubated overnight at 37˚C. Next morning, the plate was placed at 4˚C. A single colony from the plate was inoculated in 10 ml LB medium with 1% glucose and 50 µg/ml kanamycin and grown overnight at 37˚C and 250 rpm. The starter culture was added to 400 ml LB medium (with glucose and kanamycin) and grown until it reached an OD_{600} of approximately 0.6. After cooling down on ice, the culture was induced with 0.1 mM IPTG overnight at 22˚C and 250 rpm. Two-hundred ml aliquots were harvested by centrifugation at 4000g for 20 min at 4˚C and subsequently frozen at -20˚C. Two tubes with 1 ml each were harvested the same way for further analysis. For these samples, the pellet was resuspended in 300 µl cold PBS and sonicated for 6 x 15 sec. After centrifugation (15 min at 10 000 rpm and 4˚C), the supernatant was transferred to a new tube and the pellet was resuspended in 300 µl PBS. Ten µl of the samples were mixed with 4 µl loading buffer and 1.6 µl reducing agent, and analysed by gel electrophoresis. The gel was stained by SimplyBlue SafeStain (Chapter 4.4.2).

4.10.2 Protein purification

Affinity and gel filtration purification of MBP-SCHAD was performed by Kelly Velasco and is therefore described in the Appendix. Fractions of interest were analysed by SDS-PAGE (Chapter 4.4.1) and SimplyBlue SafeStain (Chapter 4.4.2).

4.10.3 SCHAD enzymatic activity assay

The enzymatic activity of the purified MBP-SCHAD variants was measured with acetyl-CoA as a substrate and NADH as a cofactor. SCHAD catalyses the reversible NAD^+-dependent dehydrogenation of 3-hydroxyaxyl-CoA to β-ketoacyl-CoA. Both NAD^+ and NADH has an absorbance maximum at 260 nm, but only NADH has a maximum at 340 nm. The activity of SCHAD can most easily be estimated in the reverse reaction by measuring the decrease in absorbance at 340 nm, as shown in Figure 4.2. The assay buffer was prepared as shown in Table

4.14. NADH was added to the buffer after measuring the blank. The absorbance at 340 nm was measured in a UV-visible wavelength spectrophotometer at 37˚C. Purified protein (0.07 µg) was added to 1 ml of the assay buffer, and measurements were made every 30 seconds for 5 minutes.

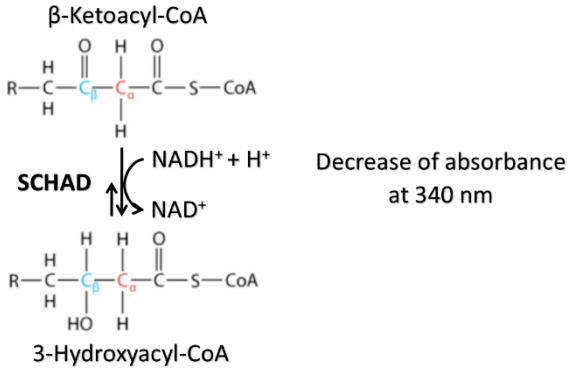

Figure 4.2 – SCHAD activity. The activity of SCHAD can be measured by the decrease of absorbance at 340 nm. NADH, which has an absorbance maximum at 340 nm, is oxidised to NAD^+ when SCHAD catalyses the conversion of β-ketoacyl-CoA to 3-hydroxyacyl-CoA.

Table 4.14 – Components of the enzymatic assay buffer.

Components	Volume
Potassium phosphate buffer (0.1 M, pH 7.0)	14.44 ml
DTT (100 mM)	15.0 µl
BSA (30 mg/ml)	150.0 µl
Acetoacetyl-CoA (5 mM)	150.0 µl
NADH (5 mM)	420.0 µl

4.11 Co-immunoprecipitation assay

Co-immunoprecipitation (Co-IP) was used to assess the ability of the different SCHAD variants to interact with GDH. $4.8x10^6$ HEK293 SCHAD KO cells were seeded per 100 mm diameter Petri dish. Two Petri dishes were used per Co-IP assay. Ten µg of each plasmid (SCHAD-V5, Figure 4.1A; GDH, Figure 4.3) were co-transfected using the calcium phosphate method (Chapter 4.3.5.1) in both plates. Forty-eight hours post transfection, the transfection efficiency was monitored visualizing the mCherry produced by the GDH plasmid using the fluorescence microscope. The medium was removed and the cells were washed once in PBS. Thereafter, the plates were kept on ice to avoid protein degradation. Five-hundred µl cold wash/lysis buffer (supplemented with protease inhibitor) were added to each plate and incubated for 5 minutes. Cells from the two corresponding plates transfected with the same plasmids were collected in one tube. Lysates were centrifuged at 13 000 g for 10 minutes at 4˚C before collecting the supernatant and discarding the pellet.

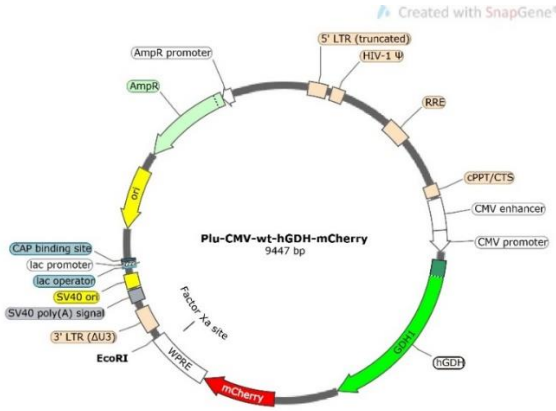

Figure 4.3 – Plasmid map of Plu-CMV-wt-hGDH-mCherry.

To capture protein complexes, a Pierce Co-Immunoprecipitation Kit was used (Figure 4.4). Co-IP was performed as described in the manufacturer's instructions, taking into account the following: Cell lysates were pre-cleared by incubation with Control Agarose Resin in a 2 ml tube for 30 minutes at 4˚C. From previous measurements, it was known that the lysates from one Petri dish usually have a protein concentration around 2 mg/ml. For pre-clearing of the cell lysate, 160 µl resin slurry was therefore used per tube. The mixture was centrifuged through a column to retain the resin, the flow-through was saved for the Co-IP, and samples were taken from the flow-through for later analysis by SDS-PAGE (input sample). Pierce Spin columns were used throughout the procedure. All resin centrifugation steps were performed at 3000 g for 30 seconds. For the Co-IP, two columns per sample were used: one used to retain the V5-tagged protein employing an anti-V5 antibody-coupled resin (V5-columns), and a second one used as a negative control containing the same kind of resin but without a coupled antibody (control columns). V5-columns were prepared as described in the instruction sheet, by coupling 10 µg of anti-V5 antibody to 50 µl AminoLink Plus Coupling Resin. According to the manufacturer, this resin contains high-yield aldehyde-activated agarose beads that covalently couples antibodies via primary amines. Control columns were prepared in the same way as the V5-columns, but omitting the addition of V5 antibody. The cell lysate containing the transfected bait (SCHAD-V5) and prey (GDH) proteins was incubated in the columns for 2 hours at 4˚C. After optimization of the manufacturer's protocol, it was decided to use a total of four washing steps before the elution. The linkage between resin and antibodies are stable during the elution conditions (non-reducing, non-denaturing). After collection of eluate 1, three additional elutions were performed to clear the resin of any remaining bound proteins so they could be re-used. Between each Co-IP procedure, resins for re-usage were stored in coupling buffer in their columns at 4˚C.

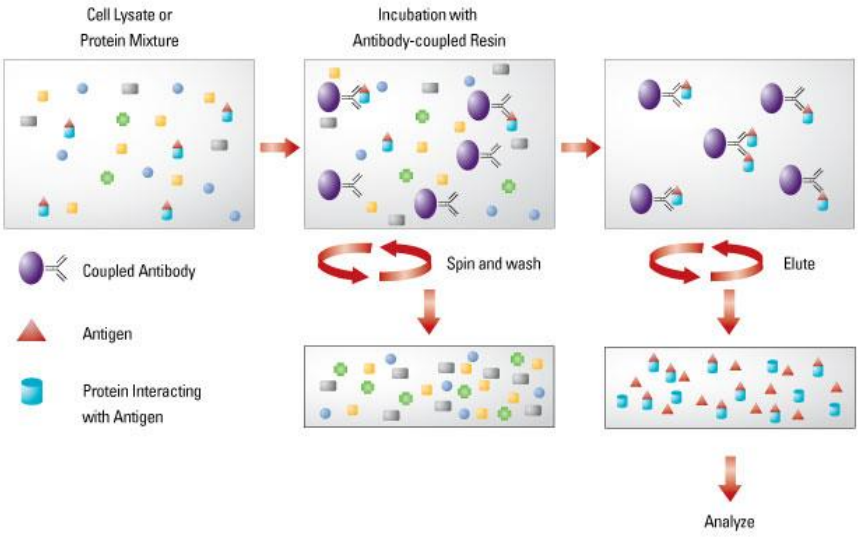

Figure 4.4 – The procedure of co-immunoprecipitation. A cell lysate is added to a column containing the antibody-coupled resin. After several washing steps, the protein complexes are eluted and the eluate is analysed by SDS-PAGE and western blotting. Protein ("prey", here GDH) interacting with the protein captured by the antibody ("bait", here SCHAD-V5) can therefore be detected. Figure from the manufacturer's protocol (Pierce).

For analysis by western blotting, samples were prepared as shown in Table 4.15. SCHAD-V5 was detected with anti-V5 antibody and GDH with anti-GLUD1 antibody.

Table 4.15 – Co-IP sample preparation for western blotting.

Components	Input	Elutions
Sample	5.0 µg	16.3 µl
4x Loading Buffer	2.5 µl	6.25 µl
10 x Reducing Agent	1.0 µl	2.5 µl
MQ H2O	To final volume of 10.0 µl	-
Final volume	10 µl	25.0 µl

4.12 Pathogenicity classification of SCHAD variants

A set of 16 different SCHAD point-mutations were interpreted by standards and guidelines from the American College of Medical genetics (ACMGM) and the Association for Molecular Pathology (AMP) (Chapter 1.4) [13]. The Alamut program was used as a support with the SCHAD reference sequence NM_005327.4 (NCBI database) chosen as reference. Alamut is a mutation analysis program used to explore and classify human genetic variants (http://www.interactive-biosoftware.com/alamut-visual/). This software collects information from several public databases (for example NCBI, EBI, UniProt and ClinVar) and includes the following in-silico tools for missense variant interpretation: PolyPhen-2, SIFT, MutationTaster and Align GVGD. SIFT predicts a substitutions effect of protein function based on the properties of the amino acid and sequence homology [64], while PolyPhen-2 predicts the impact of an amino acid substitution on both structure and function based on evolutionary considerations [65]. MutationTaster integrates data from different databases and performs analyses regarding conservation, splice-site changes, loss of protein function and changes in mRNA level [66]. Align GVGD compares the difference in biochemical properties of the original and mutated amino acid and calculate the Grantham's difference [67], which is a measure of the evolutionary distance between two amino acids [68]. Frequency data were collected from ExAC (http://exac.broadinstitute.org), GnomAD (http://gnomad.broadinstitute.org/) and 1000 Genomes databases (http://www.internationalgenome.org). The localization of the mutated amino acids were assessed to determine if the mutation affected an important functional domain or residue.

5. Results

5.1 Construction of plasmids expressing SCHAD pathogenic variants

The four variants (G34R, K136E, I184F and M188V) were chosen from case reports of patients with CHI caused by SCHAD-deficiency [16, 30, 45, 69]. To construct plasmids expressing these variants, each of the desired missense mutations were introduced into two already existing vectors expressing the wild type (WT) SCHAD protein. These vectors were pcDNA3.1-SCHAD-V5 for mammalian expression and pET-MBP-SCHAD for bacterial expression.

The eight plasmids were constructed by site-directed mutagenesis and verified by Sanger sequencing. For all plasmids, the whole reading frame of the *HADH* gene was sequenced to check that the desired mutation had been obtained, and that no other mutations had been inadvertently introduced. Figure 5.1A is a visualization of the sequencing results for one SCHAD-V5 variant (I184F). In Figure 5.1B, the sequence of the region of interest in the mutated plasmid is shown along with WT sequence, demonstrating the correct introduction of the desired mutation.

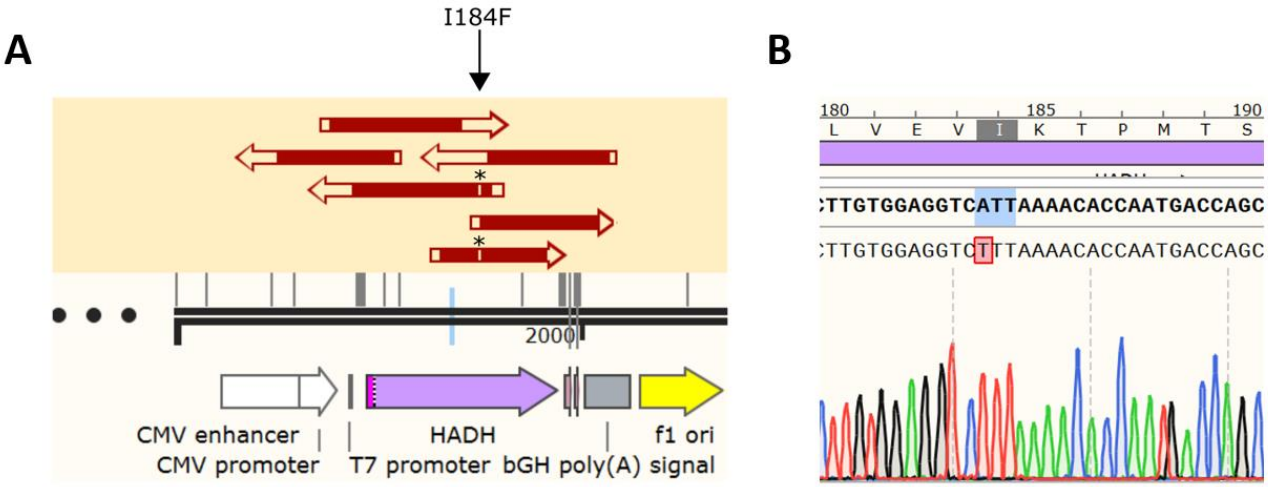

Figure 5.1 – Sequencing results verifying the construction of plasmids expressing *HADH* variants. Data from the construction of the I184F mutation in pcDNA3.1-SCHAD-V5 are shown as example. **A**) Overview of sequencing data as presented by the sequencing analysis program SnapGene. Red arrows indicate the six sequencing reaction products, each obtained with a different primer, that together cover the whole *HADH* gene (gene location shown by purple arrow). A thin, white line and star in two of the products indicate that the plasmid contains a mutation in the desired location. **B**) Nucleotide sequence of the region of interest. As shown by comparison with the WT sequence (marked in blue), the nucleotide A has been substituted by a T (red box) in position 550 of the *HADH* gene. This leads to the amino acid change I184F in the encoded protein.

Figure 5.2 shows the location of the four altered amino acids in the structure of the SCHAD protein. All of them are positioned in the NAD^+-binding domain.

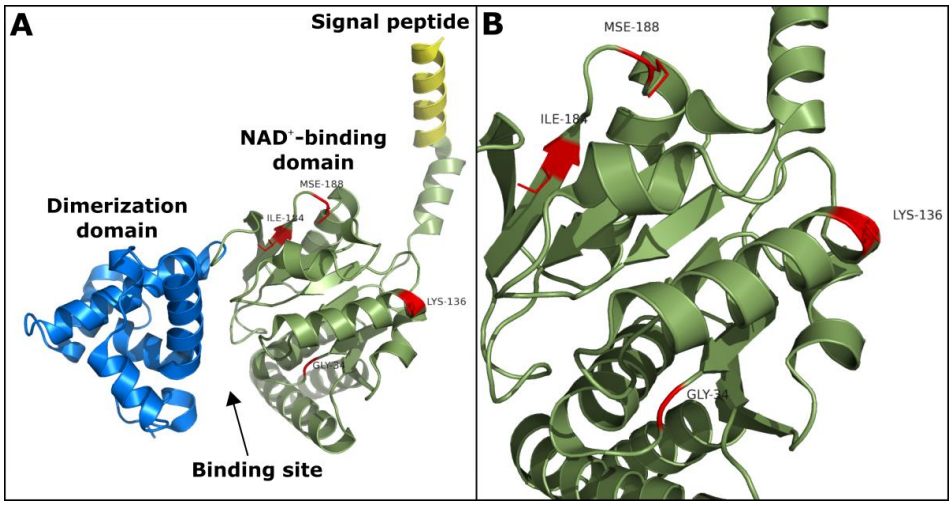

Figure 5.2 – Tri-dimensional structure of SCHAD showing how the residues G34, K136, I184 and M188 are located in the protein. A) Overall structure. Yellow = signal peptide, green = NAD^+-binding domain, blue = dimerization domain. **B)** Close-up of the NAD^+-binding domain in which all four altered amino acids are located. In the model, three letter amino acid notation has been used, and the methionine 118 has been substituted by selenomethioine (MSE). The image was obtained with the program PyMOL using the 3RQS structure of SCHAD downloaded from the protein data bank (http://www.rcsb.org/structure/3RQS)

In addition to measuring the concentration and purity of the plasmids using a NanoDrop spectrophotometer, all plasmids were subjected to electrophoresis in an agarose gel to further assess their quality. Figure 5.3 shows the separation of the SCHAD-V5 variants G34R, K136E, I184F and M188V. Restriction digestion was used to confirm that the plasmids had the expected size. As shown in the gel, the migration of the cut pcDNA3.1-SCHAD-V5 plasmids (somewhat above the 6 kb molecular weight (MW) marker) is consistent with the known size (6427 bp). For the uncut plasmids, two bands were observed, one at approximately 6500 bp and a second one weaker in intensity at the top of the gel. These two bands might correspond to a supercoiled form and a relaxed circular form of the plasmids, which in theory should have a higher and lower mobility, respectively, than the linearized form. A possibility is that the low molecular band contained a dimerization of supercoiled plasmids and therefor migrated with higher molecular weight. The further experiments (described below) confirmed that the plasmids were of sufficient quality for our purposes. The same quality control was performed for the pET-MBP-SCHAD plasmids (not shown).

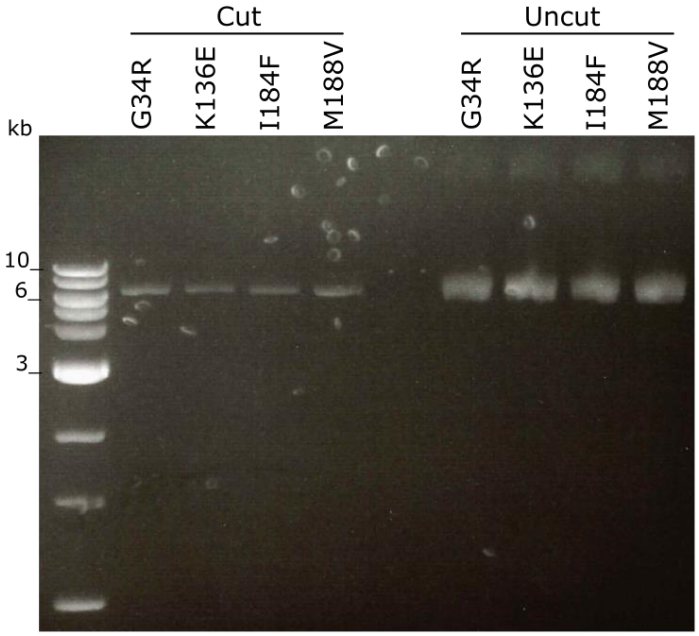

Figure 5.3 – Agarose gel electrophoresis of the pcDNA3.1-SCHAD-V5 plasmid preparations that express the variants G34R, K136E, I184F and M188V. The plasmids were digested with the restriction enzyme *Eco*RI (50 ng loaded) and compared to uncut plasmids (100 ng loaded). Plasmids were run on a 1% agarose gel stained with ethidium bromide. The left lane contains a 1 kb DNA ladder for estimating MW.

5.2 Mammalian in vitro expression of the four SCHAD variants

5.2.1 Expression in HEK293 cells and in a cell-free expression system

To test protein expression of the SCHAD variants in a mammalian cell system, the plasmids were transfected into HEK293 cells and the cell lysates were analysed by western blotting. Figure 5.4A shows expression of the pathogenic variants compared to the WT SCHAD. Cells transfected with the empty vector (pcDNA3.1 without any inserted gene) were included as a negative control. The expression was tested both in regular HEK293 cells expressing endogenous SCHAD (Figure 5.4A) and HEK293 SCHAD KO cells (Figure 5.4B) where the endogenous *HADH* gene had been disrupted (Johanna Lüdeke, unpublished). For both cell lines, a 37 kDa band corresponding to the expected MW for SCHAD-V5 could be detected when the WT, K136E and M188V plasmids were transfected. There was no SCHAD-V5 protein detected for the G34R and I184F variants.

To further test the expression of these variants, a cell-free expression system was used (Figure 5.4C). Now all variants, including G34R and I184F, were detected in similar amounts. This result shows that the plasmids expressing the G34R and I184F variants are functional, and may indicate the activity of a cellular quality control mechanism, not present in the cell-free expression system, as an explanation for the low protein levels of these variants in HEK293 cells.

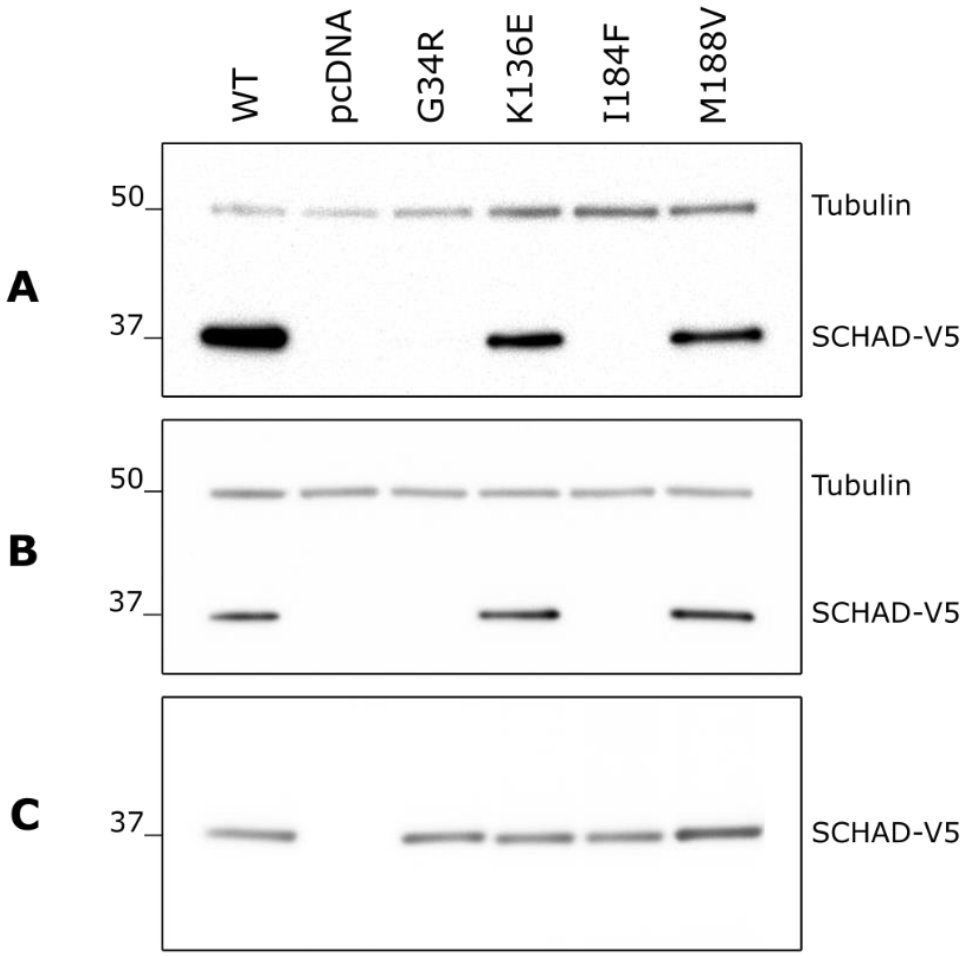

Figure 5.4 – Mammalian protein expression of SCHAD-V5 WT, G34R, K136E, I184F and M188V. A) Standard HEK293 cells were transiently transfected with SCHAD-V5 WT, pcDNA3.1 (negative control) and the SCHAD-V5 variants G34R, K136E, I184F and M188V. Cells were harvested 48 h post transfection and 2 µg cell lysate was analysed per lane by western blotting. SCHAD-V5 was detected with an anti-V5 antibody. Tubulin was used as loading control. SCHAD-V5 was detectable in the samples transfected with the WT, K136E and M188V plasmids, but not in the G34R and I184F samples. **B)** Same experiment but performed on HEK293 cells in which endogenous SCHAD expression had been knocked out by the CRISPR/Cas9 technique. The expression pattern of the SCHAD variants was similar to the ones seen for regular HEK293 cells. **C)** Western Blot of the SCHAD-V5 variants synthesized using the cell free TNT expression system. All variants now showed similar expression levels.

5.2.2 RNA expression of the *HADH* variants

Since no expressed protein could be detected for the variants G34R and I184F in HEK293 cells by western blotting, reverse transcription PCR (RT-PCR) was done to investigate the mRNA levels of these variants. HEK293 SCHAD KO cells were transiently transfected with the SCHAD-V5 variant plasmids, the empty vector (pcDNA3.1) and an additional SCHAD-V5 variant (G303S) previously constructed in the group (Kelly Velasco, unpublished). The latter was known to exhibit considerably lower protein expression than the WT, but similar levels of mRNA. It was therefore included for comparison. The cells were harvested 48 h post transfection. Total RNA was then extracted from the cells, and RT-PCR was carried out on the purified RNA. To detect *HADH* expression from the cDNA produced, primers that align to a region of the *HADH* gene and a region of the V5 tag were designed. These primers produced a 304 bp amplicon. An actin primer set that amplifies a 564 bp product was included in the reaction, and served both as positive control for the amplification and as loading control. An additional negative control using water instead of cDNA template was also included. The PCR products were separated by agarose gel electrophoresis and the results are shown in Figure 5.5. The intensity of the amplified products for the low-expression variants G34R and I184F was similar to the product for the WT. Although the method is not fully quantitative, the results suggest that the tested plasmids produce similar amounts of mRNA. Thus, the reduced protein expression of G34R and I184F is unlikely to be caused by a technical problem with the plasmids or at the transcription level, but most probably by events occurring after protein synthesis.

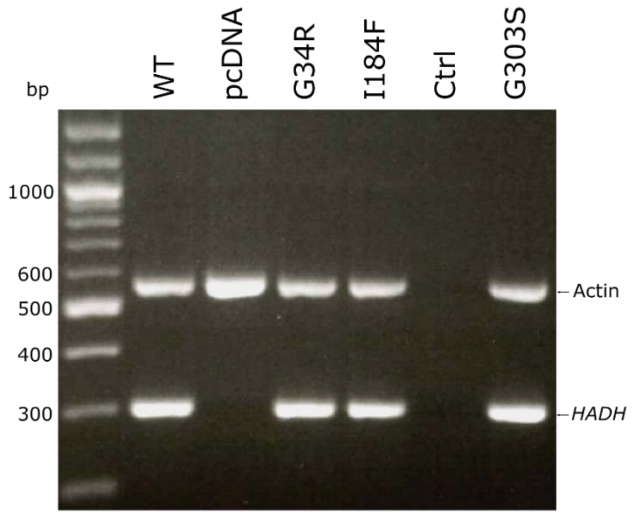

Figure 5.5 – Electrophoresis of the amplified products from cDNA using *HADH*-V5 and actin primers. HEK293 SCHAD KO cells were transiently transfected with SCHAD-V5 WT, pcDNA3.1, and the SCHAD-V5 variants G34R, I184F and G303S. Total RNA was isolated from the cell lysates 48 hours post transfection and cDNA synthesized. cDNA products were amplified with primer sets for actin and *HADH* in a duplex reaction. *HADH* product length = 304 bp. Actin product length = 564 bp. 1 kb DNA ladder to the left. Negative control: water sample (Ctrl) and pcDNA.

5.2.3 Assessment of protein expression and subcellular localization by immunofluorescent staining

Immunostaining with a fluorescent antibody and confocal imaging were done to further investigate the expression and subcellular localisation of the four constructed SCHAD-V5 variants. HEK293 SCHAD KO cells were transiently transfected with the plasmids and immunostained 48 hours post transfection. When looking at the cells at low magnification by immunofluorescence microscopy (Figure 5.6) there was a clear difference in the number of cells expressing the SCHAD protein. For the two variants K136E and M188V there were quite similar numbers of cells expressing SCHAD as for the WT protein. For G34R and I184, however, there was a considerably reduced number of cells expressing SCHAD, which confirms the data from the western blots presented in Figure 5.4. Transfection with empty vector yielded no green signal (not shown).

Figure 5.7 shows confocal images at higher magnification. When positive cells (green) for each variant were inspected, no differences could be seen as compared with cells transfected with the WT construct. The fluorescent signal co-localized with the mitochondria (red).

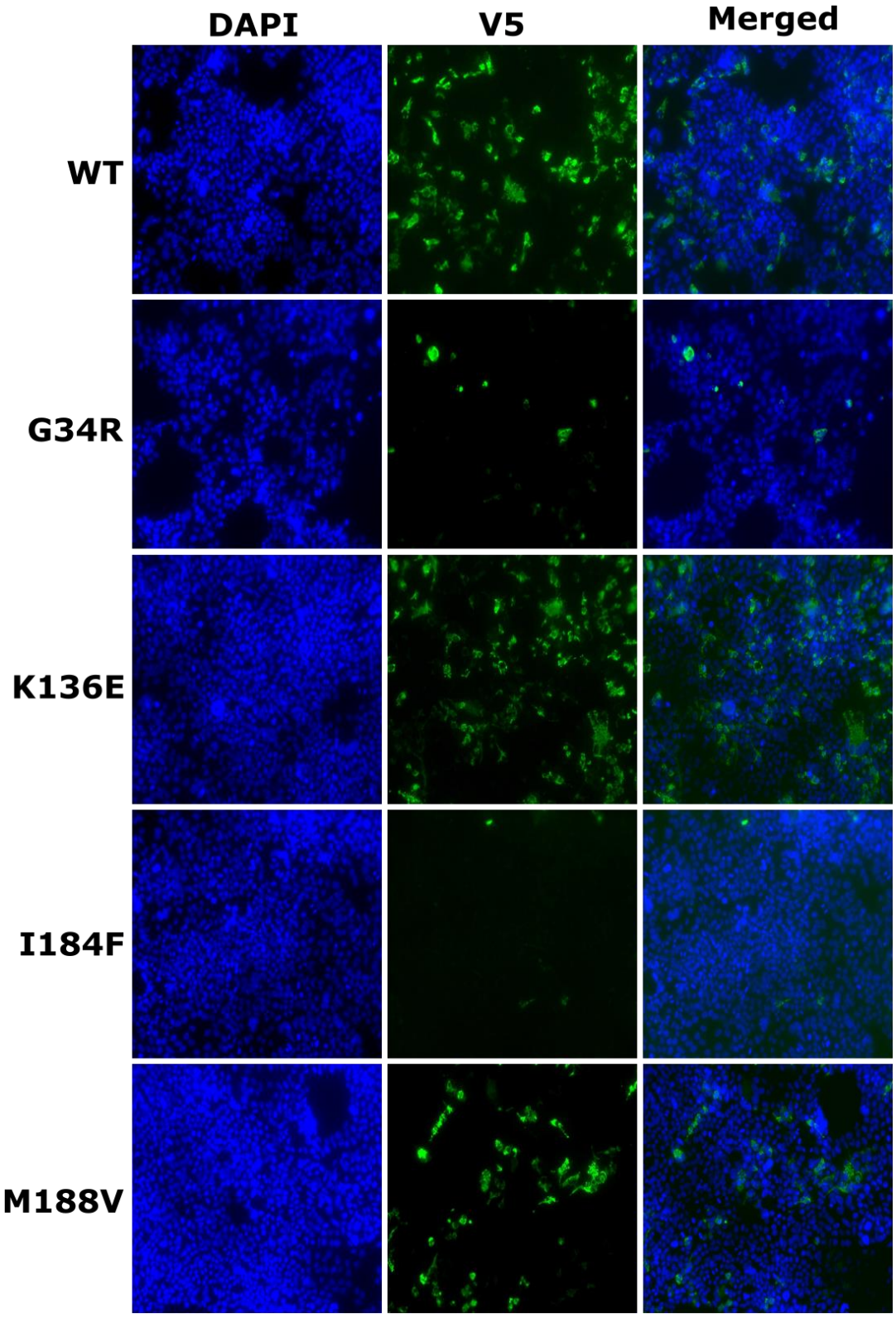

Figure 5.6 - Immuno-staining of the four SCHAD-V5 variants evaluated by fluorescence microscopy. HEK293 SCHAD KO cells were transiently transfected with the SCHAD-V5 WT, G34R, K136E, I184F and M188V plasmids. Cells were immunostained 48 hours post transfection. Fluorescence microscope images taken with a 20x objective (= 200x magnification). DAPI = blue. Primary antibody = anti-V5. Secondary antibody = AlexaFlour 488 (green).

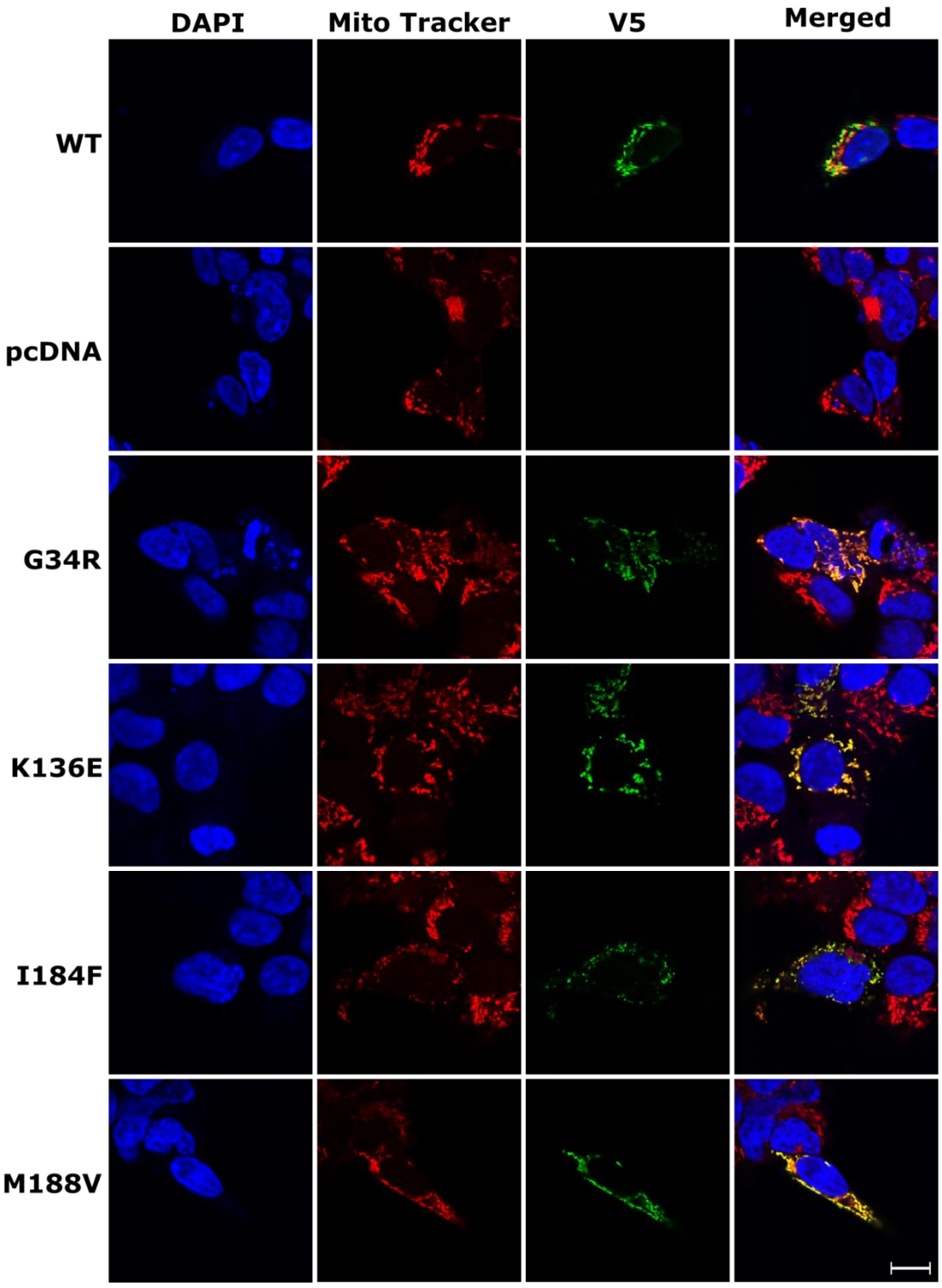

Figure 5.7 – Immuno-staining of the four SCHAD-V5 variants and of mitochondria evaluated by confocal microscopy. HEK293 SCHAD KO cells were transiently transfected with the SCHAD-V5 WT, G34R, K136E, I184F and M188V plasmids. Transfection with pcDNA3.1 was included as a negative control. Cells were immunostained 48 hours post transfection. Confocal images were taken with 63x objective plus 4x zoom. DAPI = blue. Mito Tracker = red. Primary antibody = anti-V5. Secondary antibody = AlexaFlour 488 (green). Scale bar = 10 μM.

5.2.4 Protein stability of SCHAD-V5 variants

The data obtained so far strongly suggested that protein stability was reduced for two of the pathogenic SCHAD variants (G34R and I184F). To investigate whether protein instability could be a common feature of rare SCHAD variants, a set of cycloheximide chase assays were conducted. Cycloheximide is an agent that inhibits protein synthesis. We did not include the variants G34R and I184F as they were undetectable on western blots (see Figure 5.4). Instead, we analysed the remaining two variants (K136E, M188V) together with 11 other rare SCHAD variant constructs previously made by the group (Kelly Velasco, unpublished). HEK293 SCHAD KO cells were transiently transfected with SCHAD-V5 constructs as before. Forty-eight hours after transfection the cell medium was removed and fresh medium containing cycloheximide was added to the cells. Cells were then harvested at four different time points: 0 h, 2 h, 8 h and 24 h after cycloheximide addition. Protein concentration of the cell lysates were measured, and 1 μg of each sample was analysed by SDS-PAGE and western blotting (Figure 5.8).

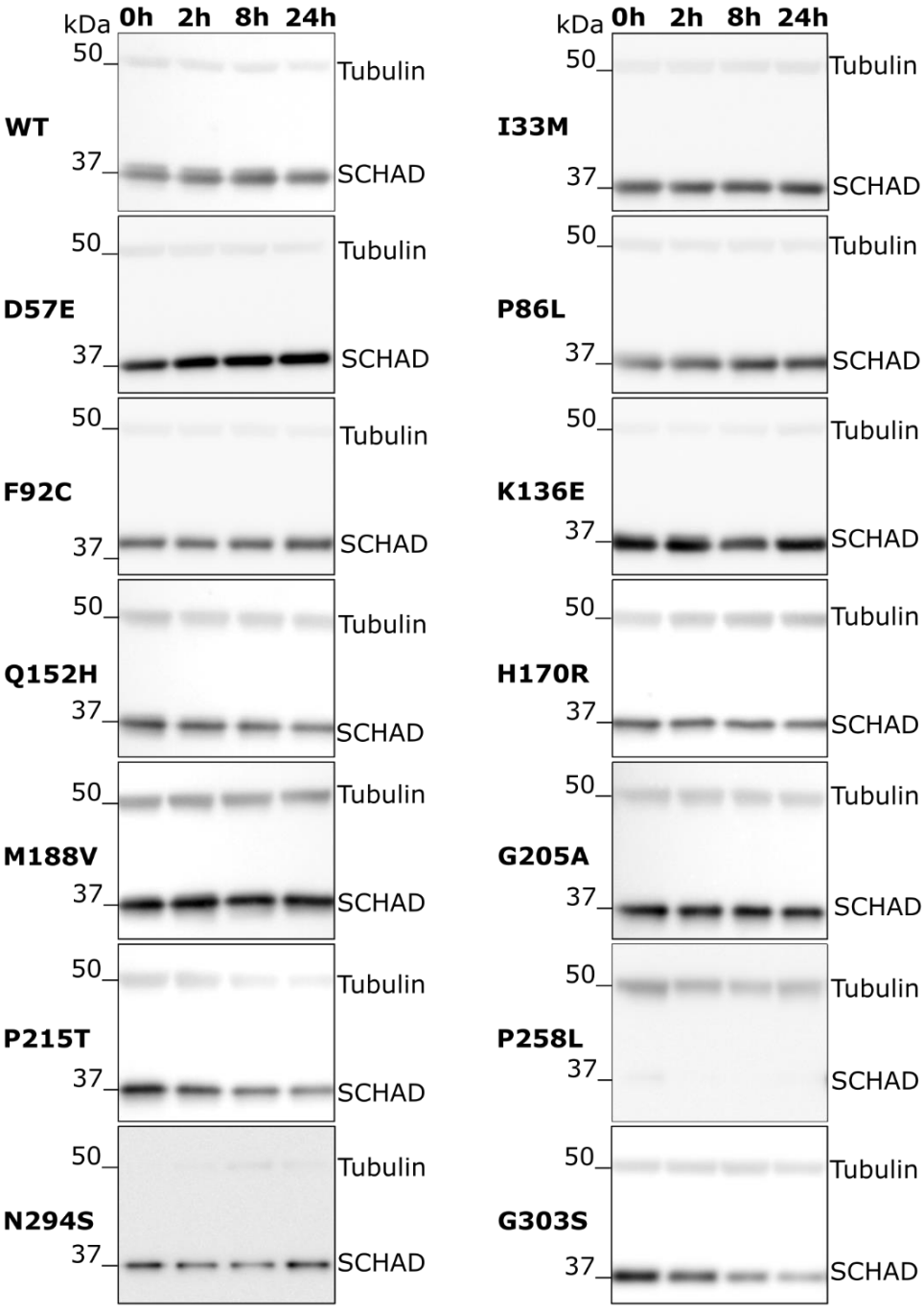

Figure 5.8 – Assessment of SCHAD-V5 variant protein stability by cycloheximide chase assay. HEK293 SCHAD KO cells were transfected with SCHAD-V5 WT and 13 rare SCHAD variants. Cells were treated with cycloheximide 48 hours post transfection and harvested at four different time points: 0 h, 2 h, 8 h and 24 h. SCHAD-V5 (37 kDa) was detected by anti-V5. Tubulin (50 kDa) was used as a loading control. For WT, H170R and G303S, representative images from two experiments are shown. The other variants were studies in one experiment only.

The amount of each SCHAD-V5 variant detected was quantified and normalized by dividing the signal of the SCHAD-V5 band by the signal of the corresponding tubulin band. This was done to compensate for potential differences in the loading of the gel and in the transfer to the membrane. P258L was almost fully degraded already at the 0 h time point, and at the 24 h time point no protein could be detected. A gradual degradation of SCHAD (normalized to tubulin) could be detected for three of the variants: I33M, H170R and G303S (Figure 5.9). There was 24%, 52% and 56% less SCHAD protein after 24 hours than at the 0 h point, respectively.

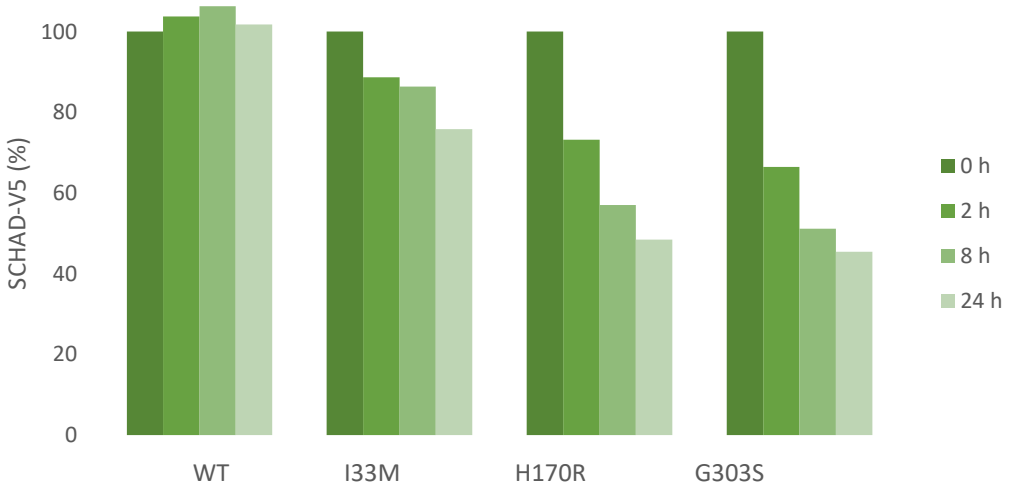

Figure 5.9 – Quantification of results from cycloheximide chase assay. A gradual decrease of the SCHAD-V5 levels (normalized to tubulin) could be detected for I33M, H170R and G303S. The protein levels at each time point are shown relative to the amount of each variant at time 0 h (100%).

5.3 Interaction of the SCHAD-V5 variants with the GDH protein

A previous study suggested that SCHAD serves as an inhibitor of the enzyme glutamate dehydrogenase (GDH) [38]. We therefore decided to test the interaction between this protein and the different SCHAD variants by co-immunoprecipitation (Co-IP). HEK293 SCHAD KO cells were co-transfected with a plasmid expressing the human GDH protein and the various SCHAD-V5 plasmids. In addition to the two pathogenic variants K136E and M188V that were stable enough to be detected on western blots (Figure 5.4), we included seven of the other rare variants available in the group. V5-antibody was covalently coupled to an amine-reactive resin packed in a column, and 48 hours after transfection the cellular lysate was run on the column to capture the V5-tagged protein. If GDH (target protein, "prey") interacted with the V5-tagged SCHAD variant ("bait" protein, captured on the column), it would be indirectly captured. The interaction complexes were eluted and analysed by SDS-PAGE and western blotting.

Before starting the set of experiments, the procedure described by the manufacturer of the Co-IP kit was optimized using cell lysates containing WT SCHAD-V5 to determine the minimum amount of washes needed to get rid of all unbound proteins of the cellular lysates. The third and fourth wash after incubation of the cell lysate in the column were collected and analysed by SDS-PAGE (Figure 5.10A). While there were still several protein bands visible after three washes, no bands appeared after four. It was therefore decided to use four washing steps. An additional washing step with conditioning buffer (wash X) suggested by the manufacturer was also tested to see if this could improve the results. No differences were observed and therefore this step was not included in the optimized protocol.

Since the V5-antibody is covalently coupled to the resin, the Co-IP columns could be reused. It was therefore important to find the required number of elutions at the end of the experiment to completely clean the column before starting a new round of Co-IP. Elution number four and five were collected for comparison (Figure 5.10B). No improvements were observed after the fifth wash, and four elutions were therefore considered sufficient.

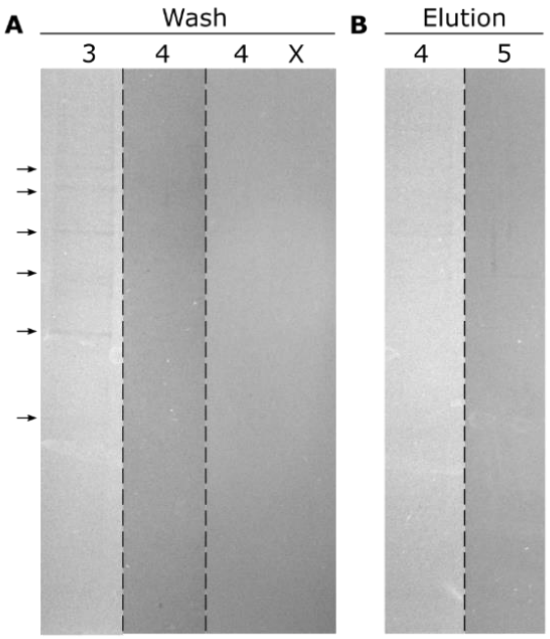

Figure 5.10 – Optimization of Co-IP protocol. **A**) Samples from the third and fourth wash steps were collected and analysed by SDS-PAGE and Coomassie staining. Note remaining weak protein bands after the third washing step (arrows). Wash number four was also compared to a sample from an additional washing step (X) with conditioning buffer. **B**) Optimization of number of elution steps. Elution number four and five were collected for comparison.

Altogether, GDH binding was tested by Co-IP for nine SCHAD variants and the WT protein. The results are shown in Figure 5.11. As seen in the top row, the SCHAD WT protein did capture GDH. A weak protein band in the anti-GDH IP eluate could also be detected for five of the other variants (F92C, Q152H, G205A, P215T, R221H). This suggested that the remaining variants bound GDH more weakly or not at all. However, protein bands were detected in the negative control lanes for some variants (F92C, K136E, M188V, P215T), which decreases the confidence of these results.

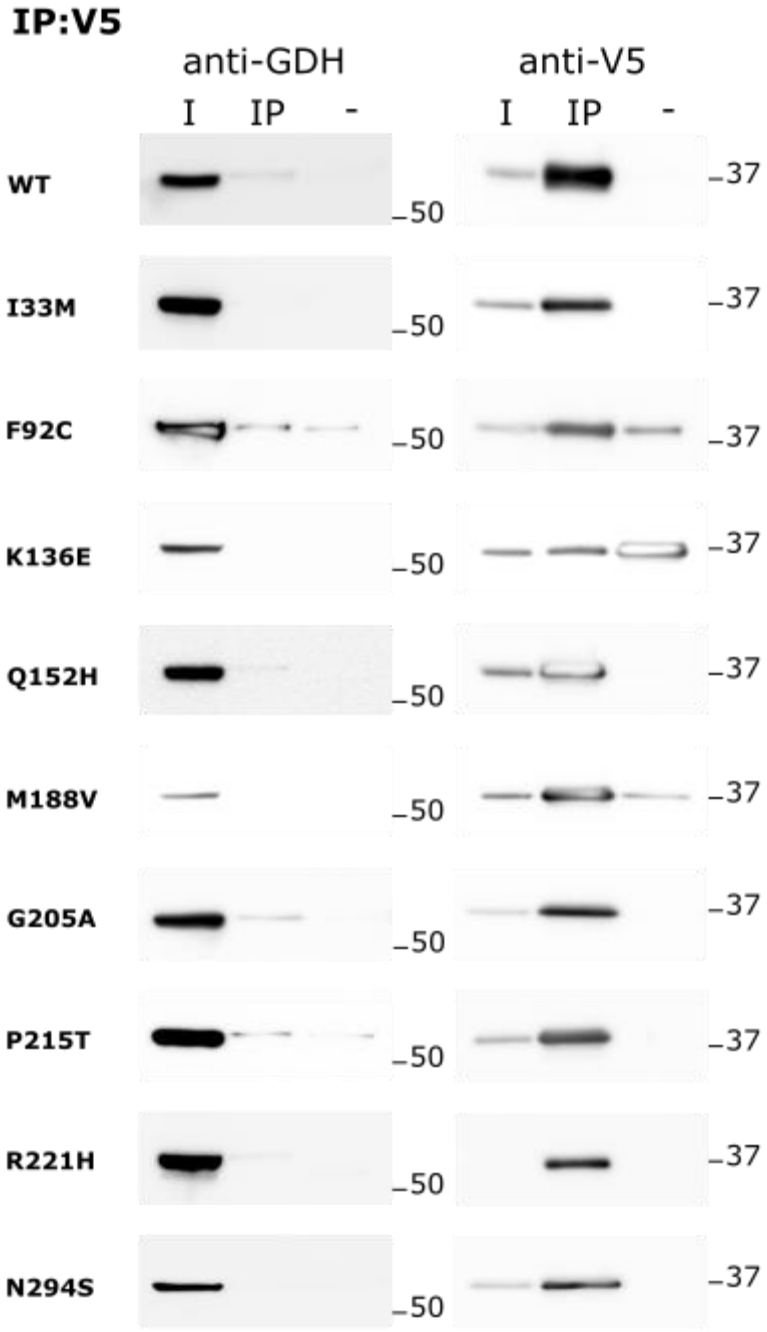

Figure 5.11 – Co-IP of GDH with SCHAD-V5. I = Input cell lysate, IP = elution from the V5-column, – = elution from the negative control column that had no V5-antibody. SCHAD (37 kD) was detected with anti-V5 and GDH (50 kD) with anti-GLUD1. Representative results from two experiments are shown.

5.4 Purification of the four SCHAD variants after bacterial expression

pET-MBP-SCHAD plasmids expressing the four variants were transformed into BL-21 *E. coli* cells and grown in culture. Protein expression was induced by adding IPTG to the growth medium. Pellet and supernatant samples from bacteria lysates were analysed by SDS-PAGE and Coomassie staining to examine whether the MBP-SCHAD protein was expressed and soluble (Figure 5.12). MBP-SCHAD had an expected size of 77 kDa (predicted using the ExPASY "Compute pI/Mw tool" https://web.expasy.org/compute_pi/), and it was known from previous experiments that protein expressed from the WT construct appears as a prominent band at approximately 75 kDa. All variants were successfully expressed and the majority of the protein was found to be soluble. A minor amount of protein was found in the pellet fraction. It looked like expression of G34R and K136E either resulted in more protein or these protein variants were more soluble than the two others. M188V had less protein in the pellet fraction, but this might have been caused by a loading problem in the gel.

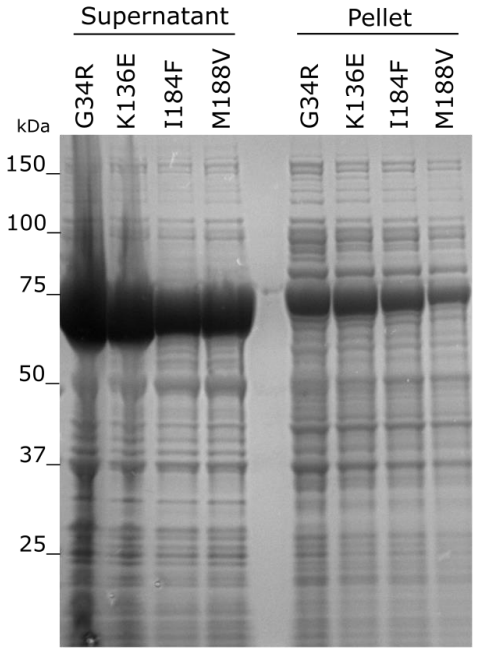

Figure 5.12 – Bacterial expression and solubility of the MBP-SCHAD variants. The pET-MBP-SCHAD variants G34R, K136E, I184F and M188V were transformed into competent *E. coli* bacteria cells. Cells were grown in LB medium with glucose, and protein expression was induced with IPTG overnight. Pelleted bacteria were suspended in PBS and sonicated. After centrifugation, samples from supernatants and pellets resuspended in equivalent volumes were analysed by SDS-PAGE and Coomassie staining.

The MBP-SCHAD variants, which also had a His-tag, were then purified from the harvested bacterial pellets from 200 ml cultures by immobilized metal affinity chromatography (IMAC, Ni-Sepharose matrix), followed by gel filtration at the Department of Biological Sciences, University of Bergen by Kelly Velasco. Figure 5.13 compares the resulting IMAC chromatograms for the different SCHAD variants. The grey line shows the elution buffer gradient. K136E and M188V eluted later compared to the WT, which could indicate a tighter binding of these variants to the Ni-Sepharose matrix. The eluted fractions containing protein, in addition to samples from supernatant, pellet and flow-through from the harvested pellet, were analysed by SDS-PAGE for verification as shown in Figure 5.14. MBP-SCHAD could be detected in several fractions for all variants.

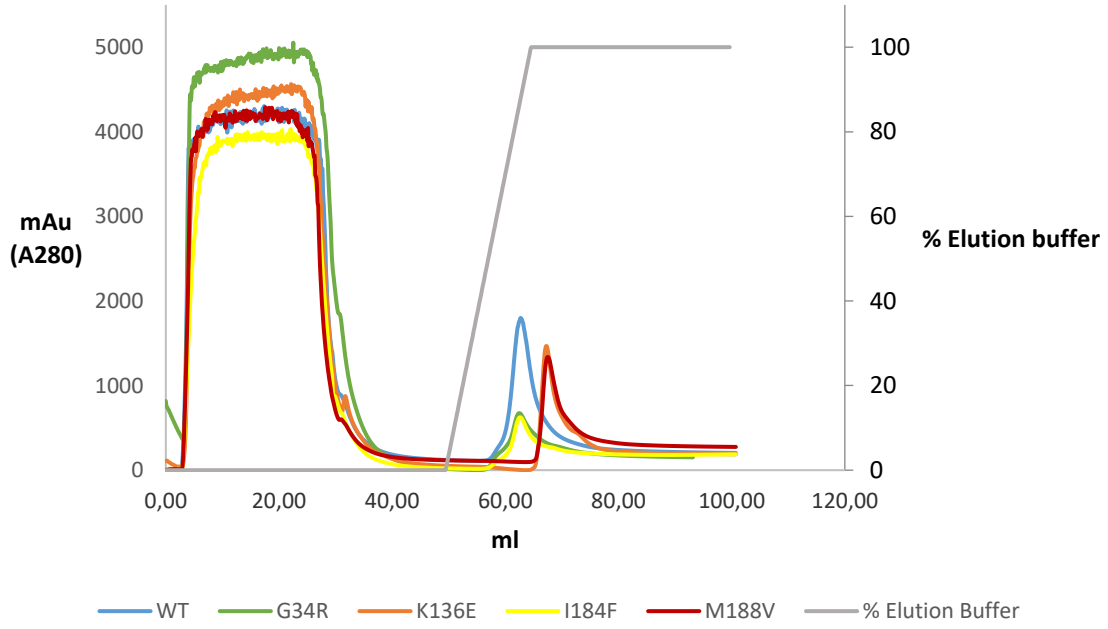

Figure 5.13 – Chromatograms from IMAC purification of the MBP-SCHAD-His WT and variants G34R, K136E, I184F and M188V. Column: HiTrap Blue HP, 5 ml. mAu = milli absorbance units at 280 nm. Data provided by Kelly Velasco.

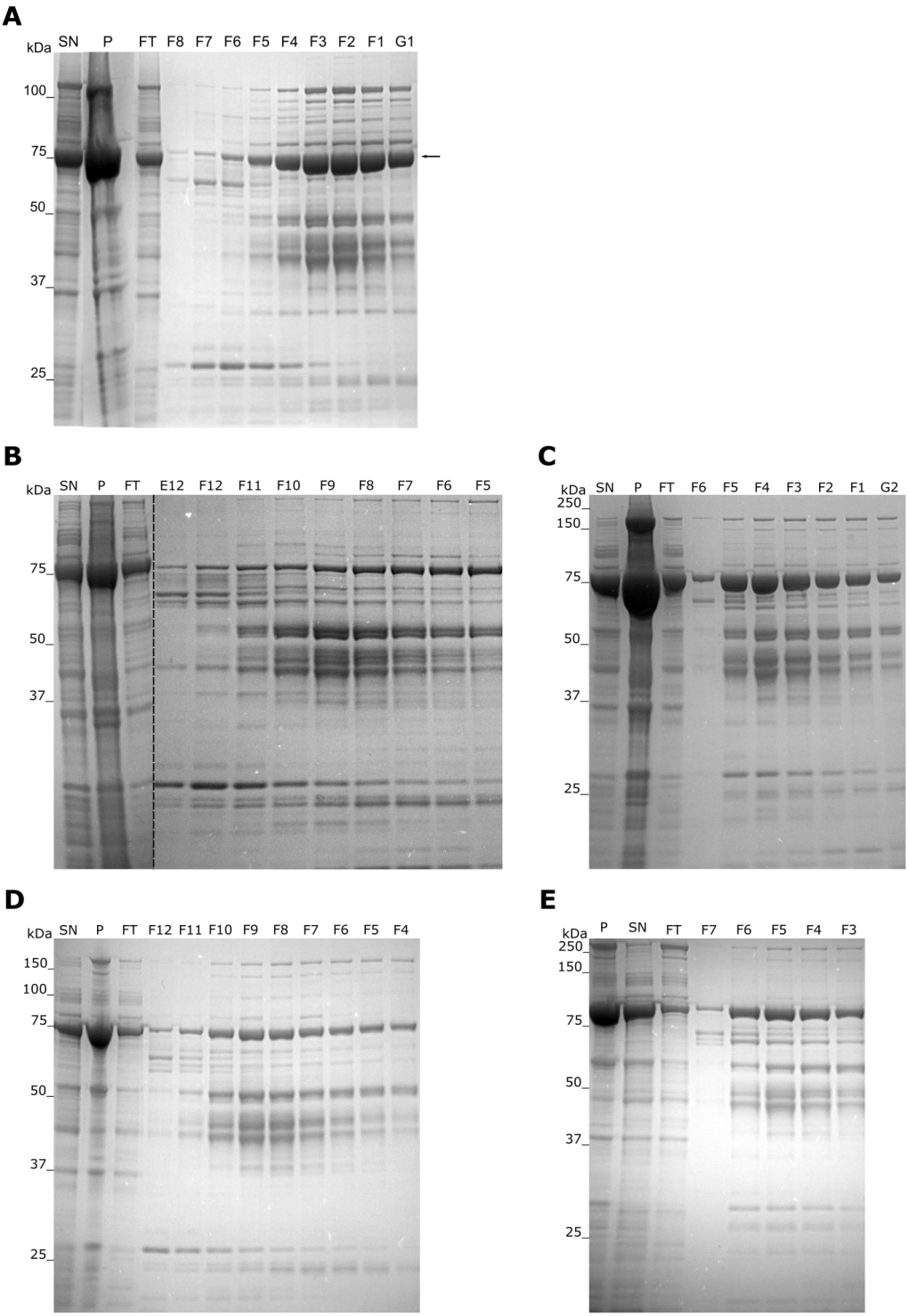

Figure 5.14 - Sampled fractions from IMAC of His-MBP-SCHAD WT and variants G34R, K136E, I184F and M188V. The samples were analysed by SDS-PAGE and Coomassie staining. SN = supernatant, FT = flow through, P = pellet. Numbers on top of the gel correspond to the various fractions tested. **A**) MBP-SCHAD WT. Arrow points to the SCHAD band. Image provided by Kelly Velasco). **B**) MBP-SCHAD G34R. **C**) MBP-SCHAD K136E. **D**) MBP-SCHAD I184F. **D**) MBP-SCHAD M188V.

However, after the IMAC step MBP-SCHAD was not considered sufficiently pure as judged from the gels (Figure 5.14). Therefore, a second purification step was needed. Fractions with the expected MW band after IMAC were pooled and purified by size exclusion chromatography (SEC, HiLoad 16/600 Superdex 200 column, performed by Kelly Velasco). From previous experiments performed in the group, it was known that dimerized MBP-SCHAD eluted in gel filtration fractions C10-D2 (Figure 5.15A). The gel filtration chromatograms are included in the Appendix (Figure A.1). The fractions collected for the four variants were then analysed by SDS-PAGE (Figure 5.15B-E). For G34R, a weak MBP-SCHAD band could be detected in the C1 fraction (Figure 5.15B), but this sample belonged to a volume eluted before the previously observed volume for the MBP-SCHAD dimers (Figure A.1) and most likely contained larger MBP-SCHAD oligomers. The amount of SCHAD in the correct fractions, as exemplified by the D10 and 11 lanes, was considered too low to continue with any experiments. For I184F (Figure 5.15D), MBP-SCHAD could be detected in all analysed fractions, but in a very low amount. For the two variants K136E (Figure 5.15C) and M188V (Figure 5.15E), SEC purification was successful. As seen from the SDS-PAGE there was a strong bad of the expected MW in the expected range for both variants and the amount was considered sufficient for further experiments, although lower than for WT MBP-SCHAD.

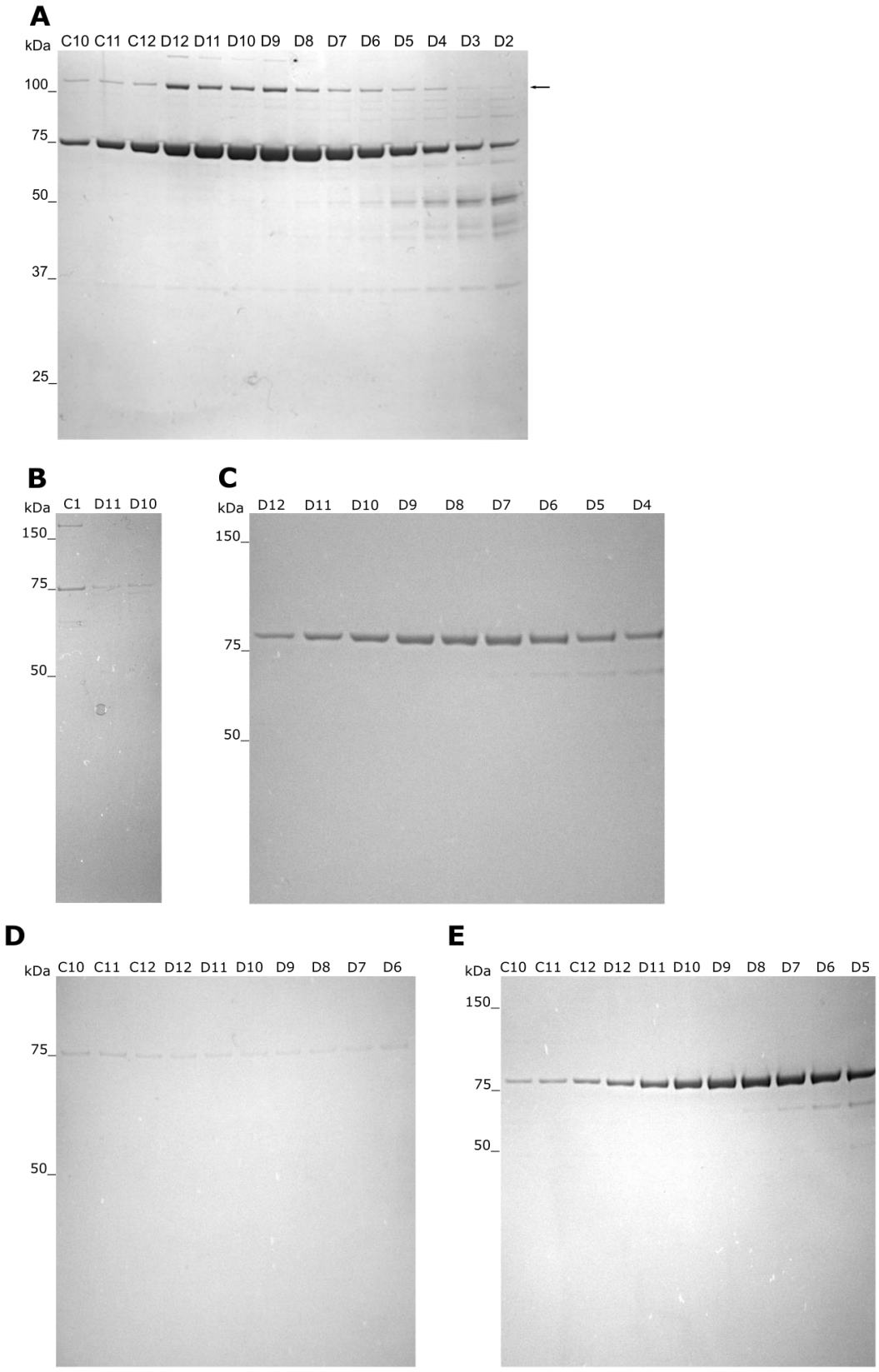

Figure 5.15 – Sampled fractions from of MBP-SCHAD-His WT and variants G34R, I184F and M188V after gel filtrations. Samples were analysed by SDS-PAGE and Coomassie staining. Numbers on top of the gel correspond to the various fractions tested. **A**) MBP-SCHAD WT (Image provided by Kelly Velasco). Note arrow pointing to the high MW band. **B**) MBP-SCHAD G34R. **C**) MBP-SCHAD K136E. **D**) MBP-SCHAD I184F. **E**) MBP-SCHAD M188V.

5.5 Enzymatic activity of MBP-SCHAD variants

The purified proteins were used to measure the enzymatic activity of the variants in comparison to the activity of WT SCHAD. The gel filtration fractions with highest concentration and purity were pooled and concentrated, and protein concentration was measured by a NanoDrop spectrophotometer. Each variant (0.5 µg and 1.0 µg) was analysed by SDS-PAGE adjacent to a WT standard ranging from 0.1-0.7 µg (Figure 5.16). The intensity of the bands could thereby be quantified compared to WT bands to account for potential impurities in the samples. After correction, the concentration of K136E (Figure 5.16A) and M188V (Figure 5.16C) was estimated to 0.22 µg/µl and 0.43 µg/µl, respectively. An additional observation for the K136E variant was that it degraded when stored at 4˚C over a period of 3-4 days (Figure 5.16B). This was not the case for WT MBP-SCHAD.

As very small amounts of I184F could be detected by SDS-PAGE (Figure 5.15D), one attempt was made to concentrate all D-fractions from the gel filtration. The concentrated sample got a final concentration under the detection limit of the NanoDrop spectrophotometer. When running the sample by SDS-PAGE, the sample appeared degraded and the protein was therefore too unstable to continue (Figure 5.16D).

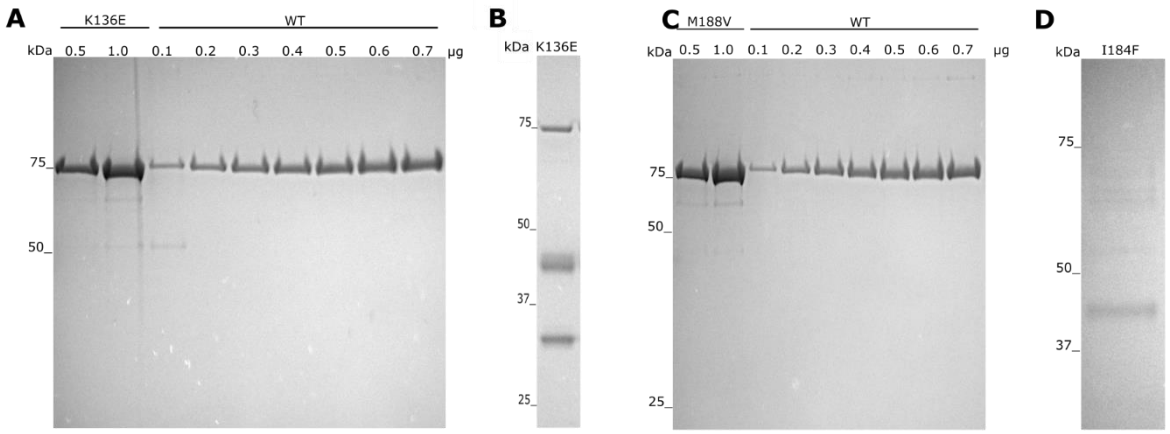

Figure 5.16 – Quantification of purified and concentrated MBP-SCHAD variants prior to the enzymatic assay. A) Quantification of the K136E variant. The concentrated sample (0.5 and 1.0 µg) from SEC fractions D12-D7 was run adjacent to a WT standard with protein concentrations ranging from 0.1 to 0.7 µg. **B**) After 3-4 days at 4˚C the MBP-SCHAD K136E was degraded. Note reduced amount of 75 kDa for K136E compared to the gel on the left and new bands at lower MW. **C**) Quantification of M188V protein concentration. Concentrated sample (0.5 and 1.0 µg) from SEC fractions D12-D6 run adjacent to WT standard. **D**) An attempt was done to concentrate the I184F fractions, but the sample was too degraded.

Since G34R and I184F could not be purified, only K136E and M188V were tested in the enzymatic assay. The measurements were done at saturated conditions of the substrate acetyl-CoA and the cofactor NADH. The results are shown in Figure 5.17. Two replicates were done for M188V and one for K136E and the WT, each one with three measurements. The enzymatic activity of K136E and M188V MBP-SCHAD was 89 µmol/min/mg and 66 µmol/min/mg respectively, whereas the WT protein had an activity of 705 µmol/min/mg. This shows that the two SCHAD variants have a severely reduced enzymatic activity.

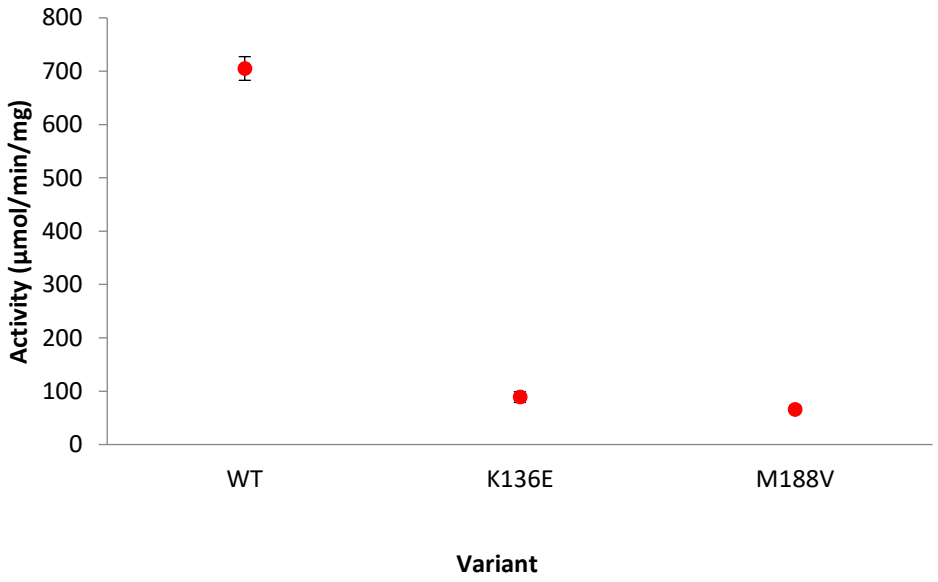

Figure 5.17 – Enzymatic activity assay for MBP-SCHAD WT and the variants K136E and MI88V. The assay was performed with 0.07 µg enzyme and substrate and co-factor saturation conditions at 37 ˚C. Two replicates were done for M188V and one for K136E and the WT, each with three measurements. The absorbance was measured at 340 nm every 30 sec for 5 min. Measured absorbance was then plotted again time. The activity in µmol/min/mg was calculated from the slope of the straight part of the curve (before the reaction reached equilibrium), using a molar extinction coefficient for NADH of 6.3 mM^{-1} cm^{-1}.

5.6 Pathogenicity classification of SCHAD variants

Finally, a reclassification was performed for the complete set of 16 rare SCHAD variants that are the focus of the group. The classification scale goes from 1, which is a benign variant, to 5, which is a pathogenic variant. The classification was done based on information about known cases from published papers, frequency data of the variants in populations, functional studies, assessment of where the mutation is located in the protein (e.g. the mutated amino acid is highly conserved and in a region important for function), and so on. For support in the classification, the software package Alamut was employed. This is a program that contains relevant information from different public databases in addition to several bioinformatics prediction tools of how protein function is altered. In the reclassification (Table 5.1), information about the functional impact of the variants, obtained by the work of this thesis, was included.

Table 5.1 – Classification of the degree of pathogenicity for SCHAD variants. Variants are interpreted by standards and guidelines from The American College of Medical Genetics and Genomics and the Association for Molecular Pathology. 1 = pathogenic, 2 = likely pathogenic, 3 = uncertain significance, 4 = likely benign and 5 = benign. * not published.

Protein AA	cDNA	Source	Exon	Domain	Frequency ExAC	Predicted class
I33M	C99G	ExAC	1	NAD-binding	0.000470	**3**
G34R	G100C	[30]	1	NAD-binding	0.000010	**5**
D57E	C171A	[56]	2	NAD-binding	0.000017	**4**
P86L	C257T	ExAC	2	NAD-binding	0.085000	**1**
F92C	T275G	ExAC	3	NAD-binding	0.005321	**3**
K136E	A406G	[69]	3	NAD-binding	-	**4**
Q152H	G456T	ExAC	4	NAD-binding	0.002026	**3**
H170R	A509G	Irish patient*	4	NAD-binding	-	**5**
I184F	A550T	[16]	5	NAD-binding	-	**5**
M188V	A562G	[45]	5	NAD-binding	-	**4**
G205A	G614C	ExAC	5	NAD-binding	0.000280	**3**
P215T	C643A	ExAC	6	Linker region	0.001674	**3**
R221H	G662A	ExAC	6	Dimerization	0.001056	**3**
P258L	C773T	[31]	7	Dimerization	-	**5**
N294S	A881G	ExAC	8	Dimerization	0.002216	**3**
G303S	G907A	[62]	8	Dimerization	-	**5**

6. Discussion

Recessive *HADH* mutations are a rare but important cause of CHI. Since SCHAD deficiency was established as a cause of CHI [33, 38], it has been an aim of our research group to fully understand the molecular basis of the phenotypic effect. In a previous study, 12 rare SCHAD variants have been functionally characterized (Kelly Velasco, unpublished data). Eight of these variants were chosen from the ExAC database. The chosen variants were rare point mutations present in human populations that resulted in amino acid substitutions and that were distributed throughout the protein. The remaining four variants were chosen from case reports of patients with CHI due to *HADH* mutations. During the initial study, it was realised that addition of more variants reported as pathogenic would strengthen the overall data. Thus, the rationale behind the current thesis was to complement the ongoing project on SCHAD biology by including four new variants found in CHI patients. After searching through the literature, the following variants were identified in recent publications: G34R, K136E, I184F and M188V.

In the present study, we examined the effect of these four new missense mutations with regard to protein expression, subcellular localization and enzymatic activity. We also expanded the earlier studies by investigating the protein stability and GDH interaction, which had not been studied for any of the variants. Thus, in some of our experiments we included all SCHAD variants[1] available in the lab, 16 in total.

6.1 About the newly selected SCHAD variants

The four new variants were all chosen from case reports of CHI patients. The G34R variant was reported by Snider et al. in 2013, and found in a patient responsive to diazoxide [30]. No other information was available about this patient. K136E was identified in a patient from Turkey by Flanagan et al. in 2011. The patient was diazoxide-responsive and had normal levels of acylcarnitines and urinary organic acids [69]. I184F was identified in two Indian sisters by Satapathy et al. in 2016. The sisters had recurrent episodes of seizures and hypoglycaemia, hyperinsulinemia and mild hyperammonemia [16]. M188V was identified in a patient from Bangladesh by Kapoor et al. in 2009. No abnormal levels of acylcarnitines and urine organic acids were detected, but the patient had a significantly decreased SCHAD activity compared to controls. The patient was responsive to diazoxide, but was severely protein sensitive and

[1] For simplicity, the full name of the expression vectors will not be used in the Discussion. SCHAD when expressed in HEK293 cells = SCHAD-V5-His. SCHAD when expressed in bacterial cells = His-MBP-SCHAD.

continued to have episodes of hypoglycaemia [45]. All the four variants were homozygous in the patients, and the clinical findings were consistent with the CHI phenotype caused by *HADH* mutations. There were therefore good reasons to consider the variants as being causative of the disease.

6.2 Expression and subcellular localization of SCHAD variants in mammalian cells

To complement the previous study done by the group, we investigated the effect of the new variants on protein expression and subcellular localization in HEK293 cells. When testing the protein expression of the SCHAD variants by western blot analysis, the two variants K136E and M188V were detected in similar amounts as the WT protein (Figure 5.4 A and B). For the two variants G34R and I184F, however, there was either no expression or expression levels were under the detection limit of the method. We also tested the expression of the four variants in a cell-free expression system. Here, all the variants were expressed in similar amounts as the WT (Figure 5.4 C). This discards any technical problem with the low-expressed plasmids, and points instead to degradation of these variants through a quality control system present only in cells. This was further supported by the results from RT-PCR (Figure 5.5), which showed similar levels of mRNA for all the variants. Even though this technique only gives an approximate estimation of the mRNA levels, these data suggest that the quality control event is most likely happening at the protein level, downstream of transcription. For a more precise quantification, quantitative real time PCR (qPCR) could have been used.

In agreement with the western blot results, immunostaining of transfected HEK293 cells showed lower fluorescent levels, though not fully absent, of the SCHAD variants G34R and I184F when compared to K136E, M188V and the WT protein (Figure 5.6). At low magnification levels it seemed like there were only a few cells expressing G34R and I184F, but a closer inspection revealed that many cells had very low expression levels (detectable at high magnifications), while very few cells had similar expression levels as the cells transfected with the WT constructs. Thus, in a few cells, these variants were apparently able to escape quality control. One hypothesis is that the positive cells are in a stage of the cell cycle where protein degradation pathways are less active or down-regulated. This is, however, only a speculation and further experiments will be needed to find the explanation. Notably, for all variants the protein was expressed in the expected subcellular localization, i.e. in the

mitochondria (Figure 5.7). This is not surprising, since none of the variants affect the N-terminal signal peptide sequence that directs the protein to the mitochondria.

Very few studies have tested the level of expressed SCHAD missense variants in cells from patients. Two of the variants that have been investigated in this regard are P258L (Clayton et al. 2001) and G303S (Vilarinho et al. 2012). Western blot analysis of patient fibroblasts revealed slightly decreased expression of P258L [62], whereas G303S had undetectable levels of expression [31]. In accordance with this data, work done in our group (Kelly Velasco, unpublished data) showed reduced protein expression of these variants in HEK293 cells, and overall very similar results to what described in this thesis for the G34R and I184F variants. G303S was also included in the RT PCR as shown in Figure 5.5. Since our test systems worked well for P258L and G303S, we consider it likely that the CHI patients carrying the G34R and I184F variants have reduced SCHAD protein levels. Likewise and interestingly, the patients carrying the K136E and M188V variants may have normal SCHAD levels, indicating that a deficiency of the protein cannot explain the disease.

All in all, protein degradation leading to too low SCHAD levels are likely to cause the disease in some cases of CHI due to *HADH* mutations. In accordance with this assumption, several of the mutations identified in patients are frame shifts or disrupt splice sites, which will lead to a truncated and/or missing SCHAD protein [34]. For other mutations, such as K136E and M188V, this is apparently not the case. Most likely, there are other defects in these variants that make them pathogenic.

6.3 Stability of SCHAD variants in mammalian cells

To further evaluate protein stability of the other available SCHAD variants, a cycloheximide chase assay was performed in transiently transfected HEK293 SCHAD KO cells. The SCHAD WT protein is very stable, and the intensity of its signal did not seem to decrease up to the last time point measured (24 hours) after treatment with cycloheximide. Among the SCHAD variants tested, I33M, H170R, P258L and G303S showed decreasing levels when normalized against a tubulin control (Figure 5.9).

We conducted the assay only once, and many technical challenges appeared during blotting and quantification. As illustrated by the WT, the protein level was not completely stable from 0 h

to 24 h (Figure 5.9), and it actually looked like it increased at the 2 h and 8 h point. Several of the other variants (e.g. D57E, P86L, K136E) also gave inconsistent results, e.g. the signal appears stronger with time or it fluctuated. The reasons for this can range from differences in transfection efficiency and cell viability, to lack of uniformity during detection. The normalization performed with the quantification of the western blot signal solves technical problems regarding protein concentration measurements and gel loading. It would also account for detection problems as long as the loading control has the same defect as its corresponding SCHAD band. This worked well for the P215T variant, which looked unstable at first glance (Figure 5.8), but after the quantification and normalization there was no decrease over time. Replicates of the cycloheximide experiment should decrease the effect of the potential errors on the final results, and will allow us to perform a statistical analysis.

The loading control tubulin was very weak in several of the blots, which made quantification difficult. Nevertheless, the variant G303S showed a very clear gradual protein degradation with a constant tubulin control. This was also the case for P258L, which was detected in very low amounts already at the 0 h time point. We are therefore confident that results from these two variants are reliable. As mentioned in Chapter 6.2, the variants G303S and P258L are pathogenic and already known to be unstable in patient samples. Degradation of the H170R variant was not obvious when looking at the blot, but after relative quantification against the tubulin control (which increased in intensity), it showed a gradual degradation similar to that of G303S. Notably, H170R is classified as pathogenic. The I33M variant had a less conspicuous rate of degradation than the aforementioned variants, but was still less stable than WT SCHAD. When purified from *E. coli* cultures, this variant degraded faster than the WT at 4°C (Kelly Velasco, unpublished), which further supports that I33M is unstable.

The cycloheximide assay might benefit from sampling at longer time points. As noted, the SCHAD protein is very stable, and it could be that the instability of some variants is only perceived at long term. After protein purification from *E.coli* the K136E variant was degraded after a couple of days storage at 4˚C (Figure 5.16B). This could indicate that the K136E protein is more unstable than the WT SCHAD, even though there was no obvious difference detected in the cycloheximide chase assay.

6.4 The effect of SCHAD variants on GDH interaction

It has been shown that SCHAD interacts with the enzyme GDH, and it is thought that SCHAD deficiency leads to CHI through the loss of the SCHAD inhibitory effect on GDH [38, 42]. This has been demonstrated by extensive analysis in *Hadh* knock out mice [38]. The aim of the Co-IP was to test whether we could replicate the in vitro interaction between the SCHAD WT protein and GDH, and investigate if the SCHAD variants had altered capacity to bind GDH. As shown in Figure 5.11, after immunoprecipitation of SCHAD WT, a GDH band appeared in the western blot, which confirmed a physical interaction between these two proteins. We therefore managed to reproduce what has been reported in literature [38, 42].

However, this assay proved technically challenging and the overall results were difficult to interpret and draw conclusions from. The most convincing results come from variants that show similar GDH binding compared to the WT. These are Q152H and G205A, which are variants with unknown significance. For the variants F92C and P215T there was bait protein (SCHAD) detected in the Co-IP column, but also in the negative control column. The negative controls, though, showed a positive signal that was less strong than the IP signals. Protein detection in the negative control experiment is likely to be caused by nonspecific binding of the protein to the coupling resin. For the pathogenic variants K136E and M188V, and the I33M and N294S variants with uncertain significance, there was no interacting GDH protein detected. Attempts were made to overexpress the signals of the blot, but still no bands were visible. This could either result from weak protein:protein interactions that cannot withstand the washing protocol, or a missing ability to interact. The results indicate that these variants bind GDH less well than the WT, but we cannot be certain since the inputs of SCHAD protein had lower signal, and the negative output therefore may be due to detection limitations.

After the assay had been performed, we realised that the low expression levels of the R22IH variant were not as expected as this variant had been stable during earlier tests. Control sequencing showed that the R221H construct had an extra mutation (p.E118Q) introduced during the in vitro mutagenesis procedure. The data for R22IH therefore have to be discarded and the experiment repeated with the correct construct.

Even though the same procedure was followed for each variant, there are several limitations in providing exactly the same conditions for each experiment, which is needed for reliable comparison. First, there might be seeding and transfection differences. Second, the columns

might not be exactly similar as each one is prepared separately in the lab. This could explain the problems with the negative controls and of uniform binding. Third, all variants cannot be blotted onto the same membrane and this could give rise to detection differences, decreasing the comparability between experiments. The first problem could be approached by using quantifiable amounts of purified protein, knowing then that the input is the same for all experiments. The second problem could be approached by preparing new columns in parallel for each Co-IP instead of reusing them. The third problem could be approached by always loading each variant next to the WT experiment, but this would increase the amount of work and materials used considerably.

6.5 Protein purification of SCHAD variants expressed in bacteria

In addition to expressing the new variants in the mammalian cell line HEK293, we also mutated the variants in a bacterial expression vector with an MBP tag (which makes the protein more soluble), transformed them into *E.coli* cells, and induced protein expression. Bacterial systems allow higher expression levels of the desired protein, in combination with lower endogenous expression of other proteins. The proteins were purified from the bacteria by IMAC and SEC. This experimental work was done in cooperation with Kelly Velasco, who handled the purification columns.

SDS-PAGE analysis of samples taken from the pellet and supernatant after lysis of the bacteria showed that for all variants there were significant amounts of the recombinant protein in the pellet fraction (Figure 5.12 and 5.14). This indicates the presence of insoluble protein. Analysing the flow-through samples from the IMAC step likewise, the M188V variant appeared to have less protein in the flow-through, which indicates a stronger binding to the column. However, we have to do more replicates to see if these trends are consistent, or if the differences are due to technical issues (bacteria handling, expression, gel loading, buffer composition, etc).

As seen in Figure 5.13, the IMAC column captured less G34R and I184F. The variants also eluted at different volumes. When gradually increasing the percentage of elution buffer added to the column, molecules that are weakly bound will be eluted first. The tendency was that K136E and M188V bound stronger to the matrix of the column, but we do not know how reproducible this is. The stronger binding of M188V corresponded to the low amount of protein in the flow-through sample for this variant, as mentioned above. The fractions containing the

SCHAD protein nevertheless still contained many contaminants (Figure 5.14) and further processing by SEC was therefore needed.

During SEC, large proteins elute first, while the small proteins are retained in the pores of the matrix and hence elute at a later volume. SCHAD WT had previously been purified several times (by Kelly Velasco), and it was already known that the protein dimer (154 kDa) should be eluted at approximately 70 ml. Even though the G34R and I184F SCHAD variants were detectable after affinity chromatography, the recovery of protein after SEC was very low. We do not know the reason, but some suggestions are: 1) The protein variants degrade fast and are so unstable that they are lost during processing. 2) The proteins are aggregating to such an extent that they are eluted from the column before they show up in the chromatogram. 3) The amount of material that we are left with after IMAC is already very low, and with the material lost during the processing stage, variants become so diluted that they cannot be detected. The purification worked well for K136E and M188V, but the recovery of purified protein was lower than for the WT (Figure A.1).

As seen in Figure 5.15A, the fractions containing the SCHAD dimers (C10-D2 fractions) also contained a band of higher molecular weight. This band probably contains other protein monomers with similar shape/volume as the SCHAD dimer. As these molecules fit in the same pores in the matrix, they cannot be separated from MBP-SCHAD by SEC.

6.6 Enzymatic activity of the SCHAD variants

Even though all four variants that were the focus of this thesis are reported as pathogenic, two of them (K136E and I184F) were expressed in similar amounts as the WT and appeared to be stable in mammalian cells. As a part of the characterization of these variants, we therefore decided to measure their enzymatic activity, comparing it with that of the WT protein. When measuring the enzymatic activity of SCHAD K136E and M188V it was found that both variants exhibited enzymatic activity, but considerably decreased compared to the WT protein (Figure 5.17). The decreased activity of M188V is in agreement with the SCHAD activity found in the patient reported by Kapoor et al. [45]. For the K136E variant there was no reported measurement of SCHAD activity [69], but both patients had normal levels of acylcarnitines and urine organic acids which indicates that there is some residual SCHAD activity. The patients with K136E and M188V mutations therefore illustrate the importance of considering SCHAD

deficiency as the cause of CHI even when no abnormalities can be detected in acylcarnitines and urine organic acids.

6.7 Formal classification of the degree of pathogenicity of rare SCHAD variants

During genetic screening of patients with inherited disorders, an increasing number of new variants of disease-causing genes are now being discovered. This is particularly true for high-throughput methods like whole-exome and -genome sequencing. The number of variants with uncertain functional significance causes problems during diagnostics of patients, and hence it is important to understand the clinical significance of a given variant. The data gathered in this study was combined with information from literature and bioinformatics tools to reclassify the total set of SCHAD variants that the group is working on. Eight of 16 variants were classified as either likely pathogenic or pathogenic, while one was classified as benign (Table 5.1). Seven of the variants were classified as of uncertain significance, as no conclusions could be drawn about their impact on SCHAD function and CHI. To be able to reach a conclusion for these variants, further studies, and preferentially with additional methods, are needed. Here, the process of classification will be explained for three of the variants: one classified as benign, one of uncertain significance, and one classified as pathogenic.

G34R, located in the NAD^+-binding domain, was reported as pathogenic by Snider et al. in 2013. [30] According to Barycki et al. 1999, the G34 residue plays an important role in the binding of cofactors to SCHAD. The NAD^+-binding site is located at the consensus nucleotide-binding motif comprised of the residues G34-G35-G36-L37-M38-G39, and is adjacent to the active site H170 which has an essential function in the catalytic mechanism [35]. The G34R mutation is predicted to be disease-causing by MutationTaster and probably damaging by PolyPhen-2. The G34 amino acid is highly conserved from *C. elegans* and there are moderate physiochemical differences between glycine and arginine. Our assays have shown that there are reduced protein levels of this variant after expression in HEK293 cells, likely due to a protein quality control mechanism. The G34R mutation is therefore classified as pathogenic.

Studies performed on the variant I33M in this thesis, in addition to an earlier unpublished study by the group, have indicated that there are some abnormalities regarding protein stability. The protein appeared to be somewhat unstable during protein purification and in the cycloheximide assay, and the Co-IP assay indicated an interrupted interaction with GDH. However, I33M has

not been previously reported as pathogenic. When analysing this variant in Alamut, the in vitro tools MutationTaster and Polyphen-2 predicted the variant to be disease causing and possibly damaging, respectively. The I33M amino acid is moderately conserved, and there is a small physiochemical difference between isoleucine and methionine (Grantham distance 10). However, our experiments are not considered sufficient to classify I33M as pathogenic, and it is therefore classified as a class 3 mutation with uncertain significance until further evidence is collected.

Polymorphisms are common variants with a minor allele frequency >1% in the population [51]. The P86L variant has a substantially higher frequency than the other variants selected for this study, and is the only common variant in the *HADH* gene that leads to a change in the amino acid composition of the protein [34]. P86L is also located in the NAD^+-binding domain. Case-control studies in the Netherlands and Denmark indicated that the minor allele frequency of SCHAD P86L varied between 6.6 and 9.2%. No significant differences in levels of circulating glucose, insulin and lipids, enzyme activity, or SCHAD protein and mRNA levels could be detected between carriers of the mutation and non-carriers. It was therefore concluded that the P86L variant had no effect on enzyme levels or function [70]. As CHI caused by SCHAD-deficiency is a very rare disease, the allele frequency of this variant strongly indicate that this variant is benign. The variant was also predicted to be benign by the *in silico* tools of Alamut, and our assays show normal protein expression in mammalian cells and no abnormalities in protein function. P86L is therefore classified as benign.

7. Conclusions

Pathogenic variants of the fatty acid oxidation enzyme SCHAD cause congenital hyperinsulinism of infancy (CHI). The overall aim of the study was to functionally characterize rare SCHAD variants, and to obtain a better understanding of how SCHAD affects insulin secretion.

The findings described in this thesis suggest that the cause of pathogenicity for the two variants G34R and I184F are protein instability, resulting in SCHAD deficiency. The variants K136E and M188V appear stable, but have impaired enzymatic activity. It has previously been postulated that the main explanation of CHI caused my mutations in the *HADH* gene is the lack of SCHAD protein [38]. Our results indicate that some pathogenic SCHAD variants are expressed at normal protein levels, but with defects in their function. Significant changes in enzyme activity are an indicator that the overall protein structure has been perturbed and that the interaction with other proteins can be severely affected. We managed to replicate the reported interaction of SCHAD WT with GDH, while a missing interaction was observed for several of the other variants.

8. Future perspectives

To finalize and extend the work described in this thesis, the following studies should be carried out:

- The cycloheximide and enzymatic assays need to be replicated. This will make it possible to perform statistical analysis, hopefully enabling conclusive results to be obtained for all variants.
- Alternative methods to evaluate the protein interaction of SCHAD and GDH need to be found. Pull-down experiments with purified proteins is one such approach, which also will help to evaluate if the interaction is direct or not.
- There is evidence that SCHAD is part of a large metabolic super complex of proteins [44]. It would therefore be very interesting to search for novel SCHAD interaction partners, for example by biochemical methods like yeast-two-hybrid screening or computational methods like network analysis.
- The effect of the SCHAD variants on the enzymatic activity of GDH should be evaluated to see if there is a varying degree of inhibition. This may aid in the evaluation of which variants are pathogenic.
- Expression of SCHAD variants were tested in HEK293 cells. A natural next step would be to evaluate the effects of SCHAD expression in a more relevant model, like directly in pancreatic beta cell lines. This would give a better indication of how the SCHAD variants directly affect insulin secretion. It wold also be interesting to investigate if rare SCHAD variants can be protective against diabetes later in life.
- It would be interesting to go through new collections of human sequence data obtained by next generation sequencing, to identify novel SCHAD variants and to investigate if we can extract more information (new variants or medical data) about the role of SCHAD in insulin regulation using tools for functional characterization established in this thesis.

References

1. Moore, K.L., A.F. Dalley, and A.M.R. Agur, *Clinically oriented anatomy*. 7th ed. ed. 2014, Philadelphia: Wolters Kluwer/Lippincott Williams & Wilkins.
2. Kumar, V., et al., *Robbins basic pathology*. 9th ed. ed. Basic pathology. 2013, Philadelphia, Pa: Elsevier/Saunders.
3. Lawlor, N., et al., *Single-cell transcriptomes identify human islet cell signatures and reveal cell-type–specific expression changes in type 2 diabetes.* Genome Research, 2017. **27**(2): p. 208.
4. Zhuo, F., R.G. Elizabeth, and L. Dongmin, *Regulation of Insulin Synthesis and Secretion and Pancreatic Beta-Cell Dysfunction in Diabetes.* Current diabetes reviews, 2013. **9**(1): p. 25.
5. Colombia University Medical Center. *The Pancreas and Its Functions*. [cited 2018 18.01]; Available from: http://columbiasurgery.org/pancreas/pancreas-and-its-functions.
6. Johns Hopkins Medicine Pathology. *Function of the pancreas* [cited 2018 18.01]; Available from: http://pathology.jhu.edu/pc/BasicOverview3.php?area=ba.
7. Nelson, D.L., et al., *Lehninger principles of biochemistry*. 6th ed. ed. 2013, New York: W.H. Freeman.
8. Lodish, H., *Molecular cell biology*. 7th ed. ed. 2013, New York: Freeman.
9. Demirbilek, H. and K. Hussain, *Congenital Hyperinsulinism: Diagnosis and Treatment Update.* Journal of Clinical Research in Pediatric Endocrinology, 2017. **9**(Suppl 2): p. 69-87.
10. Endcocrineweb. *Normal Regulation of Blood Glucose*. [cited 2018 18.01]; Available from: https://www.endocrineweb.com/conditions/diabetes/normal-regulation-blood-glucose.
11. Nessa, A., S.A. Rahman, and K. Hussain, *Hyperinsulinemic Hypoglycemia – The Molecular Mechanisms.* Frontiers in Endocrinology, 2016. **7**.
12. Kapoor, R.R., C. James, and K. Hussain, *Advances in the diagnosis and management of hyperinsulinemic hypoglycemia.* Nat Clin Pract Endocrinol Metab, 2009. **5**(2): p. 101-12.
13. The American Diabetes Association, *2. Classification and Diagnosis of Diabetes.* Diabetes care, 2018. **41**(Suppl 1): p. S13.
14. Molven, A. and P.R. Njolstad, *Role of molecular genetics in transforming diagnosis of diabetes mellitus.* Expert Rev Mol Diagn, 2011. **11**(3): p. 313-20.
15. Congenital Hyperinsulinism International. *Congenital Hyperinsulinism*. [cited 2018 19.01]; Available from: https://congenitalhi.org/congenital-hyperinsulinism/.
16. Satapathy, A., et al., *Hyperinsulinemic Hypoglycemia of Infancy due to Novel HADH Mutation in Two Siblings.* Indian Pediatrics, 2016. **53**(10): p. 912-913.
17. Thomas, P., Y. Ye, and E. Lightner, *Mutation of the pancreatic islet inward rectifier Kir6.2 also leads to familial persistent hyperinsulinemic hypoglycemia of infancy.* Human molecular genetics, 1996. **5**(11): p. 1809.

18. Thomas, P.M., et al., *Mutations in the sulfonylurea receptor gene in familial persistent hyperinsulinemic hypoglycemia of infancy.* Science (New York, N.Y.), 1995. **268**(5209): p. 426.
19. Rahman, S.A., A. Nessa, and K. Hussain, *Molecular mechanisms of congenital hyperinsulinism.* Journal of Molecular Endocrinology, 2015. **54**(2): p. R119-R129.
20. Sandal, T., et al., *The spectrum of ABCC8 mutations in Norwegian patients with congenital hyperinsulinism of infancy.* Clin Genet, 2009. **75**(5): p. 440-8.
21. Kapoor, R.R., et al., *Clinical and molecular characterisation of 300 patients with congenital hyperinsulinism.* Eur J Endocrinol, 2013. **168**(4): p. 557-64.
22. Stanley, C.A., et al., *Hyperinsulinism and Hyperammonemia in Infants with Regulatory Mutations of the Glutamate Dehydrogenase Gene.* New England Journal of Medicine, 1998. **338**(19): p. 1352-1357.
23. Stanley, C.A., et al., *Molecular basis and characterization of the hyperinsulinism/hyperammonemia syndrome: predominance of mutations in exons 11 and 12 of the glutamate dehydrogenase gene. HI/HA Contributing Investigators.* Diabetes, 2000. **49**(4): p. 667-673.
24. Sayed, S., et al., *Extremes of Clinical and Enzymatic Phenotypes in Children With Hyperinsulinism Caused by Glucokinase Activating Mutations.* Diabetes, 2009. **58**(6): p. 1419-1427.
25. Glaser, B., et al., *Familial hyperinsulinism caused by an activating glucokinase mutation.* N. Engl. J. Med., 1998. **338**(4): p. 226-230.
26. Pinney, S.E., et al., *Dominant Form of Congenital Hyperinsulinism Maps to HK1 Region on 10q.* Hormone Research in Paediatrics, 2013. **80**(1): p. 18-27.
27. Meissner, T., et al., *Exercise induced hypoglycaemic hyperinsulinism.* Archives of Disease in Childhood, 2001. **84**(3): p. 254.
28. Gonzalez-Barroso, M.M., et al., *Mutations in UCP2 in Congenital Hyperinsulinism Reveal a Role for Regulation of Insulin Secretion.* PLoS One, 2008. **3**(12).
29. Stanley, C.A., *Perspective on the Genetics and Diagnosis of Congenital Hyperinsulinism Disorders.* The Journal of Clinical Endocrinology & Metabolism, 2016. **101**(3): p. 815-826.
30. Snider, E.K., et al., *Genotype and Phenotype Correlations in 417 Children With Congenital Hyperinsulinism.* The Journal of Clinical Endocrinology & Metabolism, 2013. **98**(2): p. E355-E363.
31. Clayton, P., et al., *Hyperinsulinism in short-chain L-3-hydroxyacyl-CoA dehydrogenase deficiency reveals the importance of beta-oxidation in insulin secretion.* J. Clin. Invest., 2001. **108**(3): p. 457-465.
32. Molven, A., et al., *Familial hyperinsulinemic hypoglycemia caused by a defect in the SCHAD enzyme of mitochondrial fatty acid oxidation.* Diabetes, 2004. **53**(1): p. 221-227.

33. Molven, A., et al., *The Hypoglycemic Phenotype Is Islet Cell-Autonomous in Short-Chain Hydroxyacyl-CoA Dehydrogenase-Deficient Mice.* Diabetes, 2016. **65**(6): p. 1672-8.
34. Molven, A.H., G. Sandal, T. Njølstand, P. R. , *The Molecular Genetics and Pathophysiology of Congenital Hyperinsulinism Caused by Short-Chain 3-Hydroxyacyl-CoA Dehydrogenase Deficiency* Front Dibetes, 2012. **21**: p. 137-145.
35. Barycki, J., et al., *Biochemical characterization and crystal structure determination of human heart short chain L-3-Hydroxyacyl-CoA dehydrogenase provide insights into catalytic mechanism.* Biochemistry, 1999. **38**(18): p. 5786-5798.
36. Xu, Y., et al., *Dimerization interface of 3-hydroxyacyl-coA dehydrogenase tunes the formation of its catalytic intermediate.(Report).* PLoS ONE, 2014. **9**(4).
37. Barycki, J., et al., *Sequestration of the active site by interdomain shifting - Crystallographic and spectroscopic evidence for distinct conformations of L-3-hydroxyacyl-CoA dehydrogenase.* J. Biol. Chem., 2000. **275**(35): p. 27186-27196.
38. Li, C., et al., *Mechanism of hyperinsulinism in short-chain 3-hydroxyacyl-CoA dehydrogenase deficiency involves activation of glutamate dehydrogenase.* The Journal of biological chemistry, 2010. **285**(41): p. 31806.
39. Martens, G.A., et al., *Specificity in beta cell expression of L-3-hydroxyacyl-CoA dehydrogenase, short chain, and potential role in down-regulating insulin release.* The Journal of biological chemistry, 2007. **282**(29): p. 21134.
40. Houten, S.M., et al., *The Biochemistry and Physiology of Mitochondrial Fatty Acid β-Oxidation and Its Genetic Disorders.* Annual Review of Physiology, 2016. **78**(1): p. 23-44.
41. Vredendaal, P.J., et al., *Structural organization of the human short-chain L-3-hydroxyacyl-CoA dehydrogenase gene.* Mammalian Genome, 1998. **9**(9): p. 763-8.
42. Filling, C., et al., *Role of short-chain hydroxyacyl CoA dehydrogenases in SCHAD deficiency.* Biochemical and Biophysical Research Communications, 2008. **368**(1): p. 6-11.
43. Karaca, M., F. Frigerio, and P. Maechler, *From pancreatic islets to central nervous system, the importance of glutamate dehydrogenase for the control of energy homeostasis.* Neurochemistry International, 2011. **59**(4): p. 510-517.
44. Narayan, S.B., et al., *Short-Chain 3-Hydroxyacyl-Coenzyme A Dehydrogenase Associates with a Protein Super-Complex Integrating Multiple Metabolic Pathways (Convergence of Multiple Metabolic Pathways).* PLoS ONE, 2012. **7**(4): p. e35048.
45. Kapoor, R.R., et al., *3-Hydroxyacyl-Coenzyme A Dehydrogenase Deficiency and Hyperinsulinemic Hypoglycemia: Characterization of a Novel Mutation and Severe Dietary Protein Sensitivity.* The Journal of Clinical Endocrinology & Metabolism, 2009. **94**(7): p. 2221-2225.

46. Kapoor, R.R., et al., *3-Hydroxyacyl-coenzyme A dehydrogenase deficiency and hyperinsulinemic hypoglycemia: characterization of a novel mutation and severe dietary protein sensitivity.* J Clin Endocrinol Metab, 2009. **94**(7): p. 2221-5.
47. Owen, O.E., S.C. Kalhan, and R.W. Hanson, *The key role of anaplerosis and cataplerosis for citric acid cycle function.* The Journal of biological chemistry, 2002. **277**(34): p. 30409.
48. Pierre, M. and B.W. Claes, *Mitochondrial glutamate acts as a messenger in glucose-induced insulin exocytosis.* Nature, 1999. **402**(6762): p. 685.
49. Høy, M., et al., *Increase in cellular glutamate levels stimulates exocytosis in pancreatic β-cells.* FEBS Letters, 2002. **531**(2): p. 199-203.
50. Vetterli, L., et al., *Delineation of glutamate pathways and secretory responses in pancreatic islets with β-cell-specific abrogation of the glutamate dehydrogenase.* Molecular biology of the cell, 2012. **23**(19): p. 3851.
51. Korf, B.R. and M.B. Irons, *Human genetics and genomics*. 4th ed. ed. 2013, Chichester: Wiley-Blackwell.
52. Richards, S., et al., *Standards and guidelines for the interpretation of sequence variants: a joint consensus recommendation of the American College of Medical Genetics and Genomics and the Association for Molecular Pathology.* Genetics in Medicine, 2015. **17**(5): p. 405-423.
53. Hussain, K., et al., *Hyperinsulinism of infancy associated with a novel splice site mutation in the SCHAD gene.* The Journal of Pediatrics, 2005. **146**(5): p. 706-708.
54. Bennett, M.J., et al., *Reye-like syndrome resulting from novel missense mutations in mitochondrial medium- and short-chain l-3-hydroxy-acyl-CoA dehydrogenase.* Molecular Genetics and Metabolism, 2006. **89**(1): p. 74-79.
55. Di Candia, S., et al., *Identification of a diffuse form of hyperinsulinemic hypoglycemia by 18-fluoro-L-3,4 dihydroxyphenylalanine positron emission tomography/CT in a patient carrying a novel mutation of the HADH gene.* European Journal of Endocrinology, 2009. **160**(6): p. 1019-1023.
56. Martins, E., et al., *Short-chain 3-hydroxyacyl-CoA dehydrogenase deficiency: the clinical relevance of an early diagnosis and report of four new cases.* Official Journal of the Society for the Study of Inborn Errors of Metabolism, 2011. **34**(3): p. 835-842.
57. Flanagan, S.E., et al., *Genome-wide homozygosity analysis reveals HADH mutations as a common cause of diazoxide-responsive hyperinsulinemic-hypoglycemia in consanguineous pedigrees.* J Clin Endocrinol Metab, 2011. **96**(3): p. E498-502.
58. Fan, Z.C., et al., *Uncovering the molecular pathogenesis of congenital hyperinsulinism by panel gene sequencing in 32 Chinese patients.* Mol. Genet. Genom. Med., 2015. **3**(6): p. 526-536.
59. Babiker, O., et al., *Protein-induced hyperinsulinaemic hypoglycaemia due to a homozygous HADH mutation in three siblings of a Saudi family.(Report).* Journal of Pediatric Endocrinology and Metabolism, 2015. **28**(9 10): p. 1073.

60. Çamtosun, E., et al., *A Deep Intronic HADH Splicing Mutation (c.636+471G>T) in a Congenital Hyperinsulinemic Hypoglycemia Case: Long Term Clinical Course.* Journal of clinical research in pediatric endocrinology, 2015. **7**(2): p. 144.
61. Senniappan, S., et al., *Genotype and phenotype correlations in Iranian patients with hyperinsulinaemic hypoglycaemia.* BMC research notes, 2015. **8**: p. 350.
62. Vilarinho, L., et al., *Diagnosis of a patient with a kinetic variant of medium and short-chain 3-hydroxyacyl-CoA dehydrogenase deficiency by newborn screening.* Molecular Genetics and Metabolism, 2012. **106**(3): p. 277-280.
63. Popa, F.I., et al., *3-hydroxyacyl-coenzyme a dehydrogenase deficiency: identification of a new mutation causing hyperinsulinemic hypoketotic hypoglycemia, altered organic acids and acylcarnitines concentrations.* JIMD reports, 2012. **2**: p. 71.
64. SIFT. *SIFT*. 12.05.18 [cited 2018 12.05]; Available from: http://sift.bii.a-star.edu.sg/.
65. Adzhubei I, J.D., Sunyaev SR, *Predicting functional effect of human missense mutations using PolyPhen-2.* Curr Protoc Hum Genet 2013: p. Chapter 7:Unit7.20.
66. Schwarz, J.M., et al., *MutationTaster evaluates disease-causing potential of sequence alterations.* Nature Methods, 2010. **7**(8): p. 575.
67. National Genetics Reference Laoratory Manchester. *ALIGN-GVGD.* [cited 2018 12.05]; Available from: http://www.ngrl.org.uk/Manchester/page/align-gvgd.
68. ThermoFisher Scientific. *Grantham distance* [cited 2018 12.05]; Available from: https://ionreporter.thermofisher.com/ionreporter/help/GUID-D9DFB21C-652D-4F95-8132-A0C442F65399.html.
69. Flanagan, E.S., et al., *Genome-Wide Homozygosity Analysis Reveals HADH Mutations as a Common Cause of Diazoxide-Responsive Hyperinsulinemic-Hypoglycemia in Consanguineous Pedigrees.* Clinical Endocrinology and Metabolism, 2011. **96**(3): p. 878-878.
70. van Hove, E.C., et al., *The HADHSC Gene Encoding Short-Chain L-3-Hydroxyacyl-CoA Dehydrogenase (SCHAD) and Type 2 Diabetes Susceptibility: The DAMAGE Study*. Diabetes, 2006. **55**(11): p. 3193-3196.

Appendix

Protein purification

The frozen 200 ml bacterial pellet was resuspended in 20 ml lysis buffer with protease inhibitors without EDTA and divided in two aliquots. After 6 x 15 seconds of sonication, lysates were centrifuged at 15 000 g for 20 minutes at 4˚C. Two µl of the supernatant and the re-suspended pellet in equal volume were saved for analysis by SDS-PAGE. The supernatant was then filtrated through a 0.45 µm filter unit, and loaded into a Ni Sepharose column (HiTrap Blue HP, 5 ml) using an ÄKTAexplorer liquid chromatography system at a flow rate of 0.5 ml/min. The washing and elution were made at a flow rate of 1 ml/min. Bound protein was eluted from the column with an elution buffer gradient length of three column volumes (CV). Samples from the flow through (2 µl) and the fractions containing proteins (6 µl) were taken for later analyses by SDS-PAGE. Since the fractions containing the protein of interest had many other contaminant proteins, they were combined and further processed using a gel filtration column (HiLoad 16/600 Superdex 200 g). A sample volume ranging from 0.5 to 2.5 ml was injected at a flow rate of 0.5 ml/min. The flow rate for the rest of the run was 1 ml/min. After 0.4 CV, 1 ml fractions were collected during 0.85 CV.

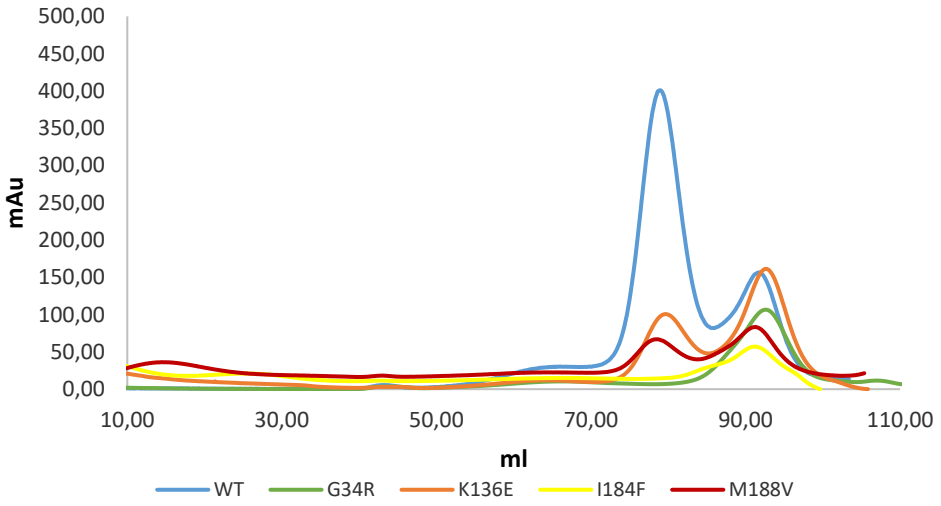

Figure A.1 – Gel filtration chromatograms from purification of MBP-SCHAD. Column: HiLoad 16/600 Superdex 200 g. mAu = milli absorbance units at 280 nm. The first peak (after 70 ml) corresponds to C10-D2 fractions in Figure 5.15A. The second peak (after 90 ml) contains molecules of lower MW. Data provided by Kelly Velasco.